ORDER RECONSTRUCTION FOR NEMATICS ON SQUARES WITH ISOTROPIC INCLUSIONS: A LANDAU-DE GENNES STUDY

YIWEI WANG, GIACOMO CANEVARI & APALA MAJUMDAR

Abstract. We prove the existence of a well order reconstruction solution (WORS)-type Landau-de Gennes critical point on a square domain with an isotropic concentric square inclusion, with tangent boundary conditions on the outer square edges. There are two geometrical parameters — the outer square edge length λ, and the aspect ratio ρ, which is the ratio of the inner and outer square edge lengths. The WORS exists for all geometrical parameters and all temperatures, and is globally stable for either λ small enough or for ρ sufficiently close to unity. We study three different types of Landau-de Gennes critical points in this setting: critical points with the minimal two degrees of freedom consistent with the imposed boundary conditions, critical points with three degrees of freedom and critical points with five degrees of freedom. We identify the competitors for the WORS in the two- and three-dimensional settings. In the three-dimensional setting, we numerically find up to 28 critical points for moderately large values of ρ, of which diagonal solutions are energy minimizing when they exist. We find two non-energy minimizing critical points with five degrees of freedom for very small values of ρ, with an escaped profile around the isotropic square inclusion.

1. Introduction. Nematic liquid crystals (NLCs) are classical examples of partially ordered materials that combine the fluidity of liquids with long-range orientational order [1, 2]. There is a substantial interest in pattern formation for NLCs in confinement, of which NLC-filled square chambers are popular examples [3, 7, 5, 6]. This paper focuses on NLC configurations inside square geometries with a square hole, referred to as an isotropic inclusion which locally destroys the surrounding nematic ordering. Such holes can be created by laser treatments or e-beam lithography techniques [48] and offer new possibilities for exciting pattern formation.

This paper is primarily motivated by the numerical and analytical results in [4] and [43], both of which focus on the WORS configuration on a square domain without a hole, within the Landau-de Gennes (LdG) theory for nematic liquid crystals. The LdG theory describes the nematic state by a macroscopic order parameter, the $\mathbf{Q}$-tensor order parameter, which is, mathematically speaking, a symmetric traceless 3×3 matrix, with five degrees of freedom. The eigenvectors of the $\mathbf{Q}$-tensor represent the preferred directions for averaged molecular alignment and the corresponding eigenvalues measure the degree of order about the eigenvectors [25, 1, 2]. In [4], the authors numerically discover a novel WORS pattern on shallow sub-micrometre scale wells with a square cross section and tangent boundary conditions oneach lateral surface. The WORS has a constant set of eigenvectors, with two eigenvectors parallel to the edges of the square and a third one orthogonal to the square, and a *defect* cross that connects the four square vertices. The corresponding $\mathbf{Q}$-tensor has two degenerate positive eigenvalues and a distinct negative eigenvalue along the diagonal cross and the molecules are locally disordered along this cross. This is referred to as a negatively-ordered uniaxial diagonal cross. The WORS is globally stable for small square domains, typically of the order of tens to hundreds of nanometers. In [43], the authors analytically prove the existence of the WORS in the same physical setting as [4]; they prove the global stability of the WORS for small square domains, the instability of the WORS for larger domains and several other qualitative results, with regards to the nature of the bifurcation etc.

In [4], the authors also numerically study the effects of a locally melted region on the WORS. For concentric square inclusions or concentric square holes (i.e. square holes that have the same centre as the domain), the WORS exists and for an off-centered square inclusion, we lose the distinctive diagonal cross and the regions of negative

uniaxiality become localised near the square edges. We take this work further in this paper and analytically and numerically study LdG equilibria on square domains with concentric isotropic square inclusions. Mathematically, this translates to a boundary value problem for the LdG $\mathbf{Q}$-tensor, with $\mathbf{Q} = 0$ on the inclusion boundary and with Dirichlet boundary conditions on the outer boundary, consistent with the experimentally imposed tangent boundary conditions in [3]. We prove the existence of a WORS-like solution for this model problem, with a constant eigenframe and a diagonal cross (along which the LdG $\mathbf{Q}$-tensor has two equal eigenvalues) that connects the vertices of the inner and outer squares, for all geometrical parameters (as described in the abstract) and for all temperatures. Following the arguments in [14] and [43], we also prove that the WORS is globally stable, i.e. is the global minimizer of the LdG energy, for either squares that are sufficiently small or for aspect ratios sufficiently close to unity. In this sense, we provide theoretical foundations for the numerical results in [4].

At a special temperature, the analysis of the WORS in [43] reduces to a scalar problem, i.e. the WORS is fully characterized by one degree of freedom. By contrast, the WORS always has two degrees of freedom (the target space is two-dimensional) in the presence of an isotropic square inclusion. The additional degree of freedom arises from the conflicting boundary conditions on the inclusion and the outer square. We perform a Γ-convergence analysis of LdG energy minimizers, in a restricted class with two degrees of freedom, in the limit of the square size $\lambda \to \infty$. The two competitors in this reduced setting are - the WORS and a critical point with two distinctive boundary layers near a pair of parallel outer square edges, referred to as the BD configuration. We compute specific minimality criteria of the WORS in terms of the material constants, temperature and geometric aspect ratio, in the $\lambda \to \infty$ limit.

The Γ-convergence analysis is complemented by a detailed numerical study of the critical points of the LdG energy for this model problem, using finite-difference based numerical methods and deflation techniques [41]. We work at the special temperature employed in [43] to reduce the number of parameters; numerical checks suggest that the results are qualitatively the same for temperatures below the nematic supercooling temperature. In Theorem 2.1, we show that LdG energy minimizers can have at most three degrees of freedom with $\hat{\mathbf{z}}$ as a fixed eigenvector, in the thin-film limit of shallow three-dimensional square wells, under appropriate assumptions. This is corroborated by the numerical investigations which show that critical points with five degrees of freedom are rare for this problem. Hence, we restrict ourselves to detailed studies of critical points with either two or three degrees of freedom. In the two-dimensional setting, the competitors have eigenvectors along the coordinate axes and are enumerated as the WORS, BD and an intermediate critical point which has half a diagonal cross. The BD and the intermediate state are never stable in the three-dimensional setting (which implies that $\hat{\mathbf{z}}$ is a fixed eigenvector of the LdG $\mathbf{Q}$-tensor but there is freedom in the (x, y)-plane), with respect to in-plane perturbations in our setting. Both the WORS and BD-configurations are stable with respect to out-of-plane perturbations. As expected, we find that the WORS is globally stable with respect to all perturbations for aspect ratios that are sufficiently close to unity i.e. narrow square annuli. In the three-dimensional setting, the WORS loses stability with respect to diagonal-type solutions (with an average molecular alignment along the square diagonals) as the square size increases or the aspect ratio decreases. We point out that our results are qualitatively consistent with the numerical results in [42] for LdG critical points with three degrees of freedom on a square without an inclusion; the main difference is that we systematically compute LdG critical points

with two and three-degrees of freedom, including unstable critical points and identify the competitors of the WORS, in the presence of an isotropic inclusion.
It is worth pointing out that the problem of LdG equilibria inside square wells has received substantial attention in recent years [3, 19, 20, 21, 4, 22, 23]. Most of them are focused on square domains without holes, e.g. [3, 19, 20] and there is some experimental/numerical work in the presence of holes[4, 22, 23, 24]. In [22], the authors study the impact of nanoparticles on LdG equilibria in square wells that have edge length comparable to the biaxial correlation length; they demonstrate exotic pattern formation induced by the nanoparticles with no overlaps with our work. The nanoparticles manifest as excluded regions for the NLC and could be viewed as *holes* in this respect. In [23], the authors study LdG equilibria within co-axial cylinders with the inner cylinder being comparable to the isotropic inclusion in our setting. In a similar vein, the authors study strong confinement of colloidal liquid crystals in a annulus-shaped microchambers by a combination of computer simulations and experiments in [24]. Numerically, it is clear that the shapes and locations of inclusions greatly enrich the solution landscape and we hope that our study, along with the others cited above, can trigger parallel experimental work in the near future.
The paper is organized as follows. In Section 2 and 3, we set up the geometric domain and the problem definition, along with recalling the mathematical framework of the LdG theory and proving the existence and uniqueness theorems for the WORS. In Section 4, we perform the Γ-convergence analysis for the limit of large domains and in Section 5, we present and analyse our numerical results. In Section 6, we briefly present our conclusions.

2. Preliminaries. The LdG theory is one of the most powerful continuum theories for nematic liquid crystals and describes the nematic state by a macroscopic order parameter — the LdG $\mathbf{Q}$-tensor that is a macroscopic measure of material anisotropy. The LdG $\mathbf{Q}$-tensor is a symmetric traceless 3×3 matrix, i.e.

$$\mathbf{Q} \in S_0 := \left\{ \mathbf{Q} \in \mathbb{M}^{3\times 3} \colon Q_{ij} = Q_{ji},\ Q_{ii} = 0 \right\}.$$

A $\mathbf{Q}$-tensor is said to be (i) isotropic if $\mathbf{Q} = 0$, (ii) uniaxial if $\mathbf{Q}$ has a pair of degenerate non-zero eigenvalues and (iii) biaxial if $\mathbf{Q}$ has three distinct eigenvalues [1]. A uniaxial $\mathbf{Q}$-tensor can be written as $\mathbf{Q}_u = s\left(\mathbf{n} \otimes \mathbf{n} - \mathbf{I}/3\right)$ with $\mathbf{I}$ the 3×3 identity matrix, $s \in \mathbb{R}$ and $\mathbf{n} \in \mathbb{S}^2$, a unit vector. The scalar, s, is an order parameter which measures the degree of orientational order. The vector, $\mathbf{n}$, is the eigenvector with the non-degenerate eigenvalue, referred to as the "director" and labels the single distinguished direction of uniaxial nematic alignment [1, 2].
In the absence of surface energies, a simple form of the LdG energy is given by [1, 2]

$$I[\mathbf{Q}] := \int \frac{L}{2} \left|\nabla \mathbf{Q}\right|^2 + f_B(\mathbf{Q}) \, \mathrm{d}A, \tag{2.1}$$

where

$$\left|\nabla \mathbf{Q}\right|^2 := \frac{\partial Q_{ij}}{\partial r_k} \frac{\partial Q_{ij}}{\partial r_k}, \qquad f_B(\mathbf{Q}) := \frac{A}{2} \operatorname{tr} \mathbf{Q}^2 - \frac{B}{3} \operatorname{tr} \mathbf{Q}^3 + \frac{C}{4} \left(\operatorname{tr} \mathbf{Q}^2\right)^2. \tag{2.2}$$

The variable $A = \alpha(T - T^*)$ is the re-scaled temperature, α, L, B, $C > 0$ are material-dependent constants and T^* is the characteristic nematic supercooling temperature [1]. Further, $\mathbf{r} := (x, y)$, $\operatorname{tr} \mathbf{Q}^2 = Q_{ij}Q_{ij}$ and $\operatorname{tr} \mathbf{Q}^3 = Q_{ij}Q_{jk}Q_{ki}$ for i, j, $k = 1, 2, 3$. All stationary points of this thermotropic potential, f_B, are either uniaxial or isotropic [1, 25]. The re-scaled temperature A has three characteristic values:

(i) the nematic supercooling temperature, $A = 0$, below which the isotropic phase $\mathbf{Q} = 0$ loses stability, (ii) the nematic-isotropic transition temperature, $A = B^2/27C$, at which f_B is minimized by the isotropic phase and a continuum of uniaxial states and (iii) $A = B^2/24C$, above which the isotropic state is the unique critical point of f_B. We work with $A < 0$, i.e. low temperatures and the numerical work in this paper focuses on a special temperature, $A = -B^2/3C$, largely to facilitate comparison with [43]. Our analytical results are true for all temperatures, $A < 0$. For a given $A < 0$, let $\mathscr{N} := \{\mathbf{Q} \in S_0 \colon \mathbf{Q} = s_+ (\mathbf{n} \otimes \mathbf{n} - \mathbf{I}/3)\}$ denote the set of minimizers of the bulk potential, f_B, with

$$s_+ := \frac{B + \sqrt{B^2 + 24|A|C}}{4C},$$

and $\mathbf{n} \in \mathbb{S}^2$ arbitrary.

We model nematic profiles on a three-dimensional square well in the limit of vanishing depth, as will be rigorously established below. More precisely, the domain is

$$\mathcal{B} = \Omega \times [0, h]\,, \tag{2.3}$$

where Ω is a two-dimensional square and we work in the $h \to 0$ limit, i.e. the limit of vanishing thickness. The underpinning assumptions are that we have Dirichlet uniaxial tangent boundary conditions on the lateral surfaces and impose finite anchoring on the top and bottom surfaces, which favours tangent boundary conditions or equivalently prefers the nematic molecules to lie in the plane of the square. The Dirichlet conditions on the sides are consistent with the tangent boundary conditions on the top and bottom surfaces.

We non-dimensionalize the system using a change of variables, $\bar{\mathbf{r}} = \left(\frac{x}{\lambda}, \frac{y}{\lambda}, \frac{z}{h}\right)$, where λ is the square edge length. The quantity hL has the dimensions of an energy and the re-scaled LdG energy is given by

$$\overline{I}[\mathbf{Q}] := \frac{I[\mathbf{Q}]}{hL} = \int_0^1 \int_{\overline{\Omega}} \frac{1}{2} \left|\overline{\nabla_{x,y}}\mathbf{Q}\right|^2 + \frac{1}{\sigma^2} \left|\overline{\nabla_z}\mathbf{Q}\right|^2 + \frac{\lambda^2}{L} f_B\left(\mathbf{Q}\right) d\bar{V} + \frac{1}{\sigma} \int_{\overline{\Omega}\times\{0,1\}} f_s\left(\mathbf{Q}, \hat{\mathbf{z}}\right)\, d\bar{S}, \tag{2.4}$$

where $\sigma = \frac{h}{\lambda}$ and f_s is a non-dimensionalized surface anchoring energy density on the top and bottom plates, which will be given later. We drop the bars from the re-scaled variables.

In what follows, we quote a result from [44] that allows us to drop the third dimension. (The reader is also referred to [45] for a more recent result, which includes the limit of small nematic correlation length.) Consider the surface anchoring energy density (see [44, Eq. (16)]):

$$f_s(\mathbf{Q}, \hat{\mathbf{z}}) = \alpha \left(\mathbf{Q}\hat{\mathbf{z}} \cdot \hat{\mathbf{z}} - \beta\right)^2 + \gamma \left|(\mathbf{I} - \hat{\mathbf{z}} \otimes \hat{\mathbf{z}})\mathbf{Q}\hat{\mathbf{z}}\right|^2, \tag{2.5}$$

where α, β and γ are constants. We assume that

$$0 < \alpha = \alpha(\sigma) \ll \sigma, \text{ so that } \frac{\alpha(\sigma)}{\sigma} \to 0, \tag{2.6}$$

$$\gamma > 0 \text{ is an } \sigma\text{-independent constant.} \tag{2.7}$$

This surface anchoring energy favours planar boundary conditions on the top and bottom plates, such that $\hat{\mathbf{z}}$ is an eigenvector of $\mathbf{Q}$ on the top and bottom plates with associated eigenvalue β. We impose a Dirichlet boundary condition, $\mathbf{Q}_b$, on the lateral surface, $\partial\Omega \times [0, 1]$ and assume that:

$$\mathbf{Q}(x, y, z) = \mathbf{Q}_b(x, y) \qquad \text{for } (x, y) \in \partial\Omega,\ z \in (0, 1) \qquad \text{and} \tag{2.8}$$

(2.9) $\hat{\mathbf{z}}$ is an eigenvector of $\mathbf{Q}_b(x, y)$ for any $(x, y) \in \partial\Omega \times (0, 1)$.

THEOREM 2.1 (Straightforward adaptation of [44], Th. 5.1). *Suppose that the assumptions (2.6), (2.7), (2.9) hold. In the limit as $\sigma \to 0$, minimisers of the functional (2.4) subject to the boundary condition (2.8) converge (strongly in H^1) to minimisers of the functional*

$$I_0[\mathbf{Q}] := \int_\Omega \left(|\nabla_{x,y}\mathbf{Q}|^2 + \frac{\lambda^2}{L} f_b(\mathbf{Q}) \right) \mathrm{d}V \tag{2.10}$$

subject to the constraint *that*

$$\hat{\mathbf{z}} \text{ is an eigenvector of } \mathbf{Q}(x, y) \qquad \textit{for any } (x, y) \in \Omega \tag{2.11}$$

and to the boundary condition

$$\mathbf{Q} = \mathbf{Q}_b \qquad \textit{on } \partial\Omega.$$

We assume that the conditions of this theorem hold. We heuristically justify this on the grounds that if $\mathbf{Q}_b$ has $\hat{\mathbf{z}}$ as a fixed eigenvector and if the surface anchoring conditions on the top and bottom surfaces of a thin well enforce a fixed eigenvector ($\hat{\mathbf{z}}$), then $\hat{\mathbf{z}}$ is expected to be a fixed eigenvector throughout the domain in (3.1). Under these assumptions, we study critical points of the reduced energy (2.10) and the associated Euler-Lagrange equations are:

$$\Delta\mathbf{Q} = \frac{\lambda^2}{L} \left\{ A\mathbf{Q} - B\left(\mathbf{Q}\mathbf{Q} - \frac{\mathbf{I}}{3}|\mathbf{Q}|^2 \right) + C|\mathbf{Q}|^2\mathbf{Q} \right\}, \tag{2.12}$$

where Δ is the two-dimensional Laplacian, $(\mathbf{Q}\mathbf{Q})_{ik} = Q_{ij}Q_{jk}$ with $i, j, k = 1, 2, 3$. In what follows, we treat A, B, C, L as fixed constants and vary λ.

3. The Variational Problem. We take the rescaled domain $\Omega \subseteq \mathbb{R}^2$ to be a truncated square with a square inclusion. For fixed $0 < \rho < 1$, we define

(3.1)
$$\Omega := \big\{(x, y) \in \mathbb{R}^2 \colon |x| < 1 - \varepsilon,\ |y| < 1 - \varepsilon,\ \rho < |x + y| < 1,\ \rho < |x - y| < 1\big\}.$$

The boundary, $\partial\Omega$, has two components, an inner boundary and an outer boundary. The inner boundary, Γ_{in}, is a square with edge length $\sqrt{2}\rho$ and whose diagonals are parallel to the coordinate axes. The outer boundary, Γ_{out}, consists of four "long" edges $C_1, \ldots, C_4$, parallel to the lines $y = x$ and $y = -x$, and four "short" edges $S_1, \ldots, S_4$, of length 2ε, parallel to the x- and y-axes respectively. The long edges C_i are labeled counterclockwise and C_1 is defined by

$$C_1 := \big\{(x, y) \in \mathbb{R}^2 \colon x + y = 1,\ \varepsilon \le x \le 1 - \varepsilon\big\}.$$

The short edges S_i are also labeled counterclockwise and

$$S_1 := \big\{(1 - \varepsilon, y) \in \mathbb{R}^2 \colon |y| \le \varepsilon\big\}.$$

The domain is drawn in Figure 3.1(a). We work with Dirichlet conditions on $\partial\Omega$, consistent with the Dirichlet conditions on the lateral sides in [44]. To mimic the isotropic inclusion, we impose *isotropic* boundary conditions on the inner boundary Γ_{in}, i.e.

$$\mathbf{Q}(\mathbf{r}) = \mathbf{Q}_{\text{b}}(\mathbf{r}) := 0 \qquad \text{for } \mathbf{r} \in \Gamma_{\text{in}}. \tag{3.2}$$

We impose *tangent* uniaxial Dirichlet conditions on the long edges, $C_1, \ldots, C_4$. We fix $\mathbf{Q} = \mathbf{Q}_\mathrm{b}$ on $C_1, \ldots, C_4$, where

$$\mathbf{Q}_\mathrm{b}(\mathbf{r}) := \begin{cases} s_+ \left(\mathbf{n}_1 \otimes \mathbf{n}_1 - \dfrac{\mathbf{I}}{3} \right) & \text{for } \mathbf{r} \in C_1 \cup C_3 \\ s_+ \left(\mathbf{n}_2 \otimes \mathbf{n}_2 - \dfrac{\mathbf{I}}{3} \right) & \text{for } \mathbf{r} \in C_2 \cup C_4; \end{cases} \tag{3.3}$$

and

$$\mathbf{n}_1 := \frac{1}{\sqrt{2}} (-1,\, 1,\, 0)\,, \qquad \mathbf{n}_2 := \frac{1}{\sqrt{2}} (1,\, 1,\, 0)\,.$$

The Dirichlet condition on the short edges is defined in terms of a function $g\colon [-\varepsilon,\, \varepsilon] \to [-s_+/2, s_+/2]$, which is chosen to eliminate discontinuities of the tangent Dirichlet boundary condition. We take g to be (the choice of g does not affect qualitative predictions or numerical results)

$$g(y) := \frac{s_+}{2\varepsilon} s, \qquad \text{for } -\varepsilon \le s \le \varepsilon$$

on S_1. We fix $\mathbf{Q} = \mathbf{Q}_\mathrm{b}$ on $S_1, \ldots, S_4$ where

$$\mathbf{Q}_\mathrm{b} := \begin{cases} g(y) \left(\mathbf{n}_1 \otimes \mathbf{n}_1 - \mathbf{n}_2 \otimes \mathbf{n}_2 \right) - \dfrac{s_+}{6} \left(2\hat{\mathbf{z}} \otimes \hat{\mathbf{z}} - \mathbf{n}_1 \otimes \mathbf{n}_1 - \mathbf{n}_2 \otimes \mathbf{n}_2 \right) & \text{on } S_1 \cup S_3, \\ g(x) \left(\mathbf{n}_1 \otimes \mathbf{n}_1 - \mathbf{n}_2 \otimes \mathbf{n}_2 \right) - \dfrac{s_+}{6} \left(2\hat{\mathbf{z}} \otimes \hat{\mathbf{z}} - \mathbf{n}_1 \otimes \mathbf{n}_1 - \mathbf{n}_2 \otimes \mathbf{n}_2 \right) & \text{on } S_2 \cup S_4. \end{cases} \tag{3.4}$$

Given the Dirichlet conditions (3.2), (3.3) and (3.4), the admissible space is

$$\mathscr{A} := \left\{ \mathbf{Q} \in W^{1,2}(\Omega,\, S_0)\colon \mathbf{Q} = \mathbf{Q}_\mathrm{b} \text{ on } \partial\Omega \right\}. \tag{3.5}$$

We look for critical points of the re-scaled functional (2.10) of the form

$$\mathbf{Q}(x,\, y) = q_1(x,\, y) \left(\mathbf{n}_1 \otimes \mathbf{n}_1 - \mathbf{n}_2 \otimes \mathbf{n}_2 \right) + q_3(x,\, y) \left(2\hat{\mathbf{z}} \otimes \hat{\mathbf{z}} - \mathbf{n}_1 \otimes \mathbf{n}_1 - \mathbf{n}_2 \otimes \mathbf{n}_2 \right) \tag{3.6}$$

subject to the boundary conditions

$$q_1(x,\, y) = q_{1,\mathrm{b}}(x,\, y) := \begin{cases} 0 & \text{on } \Gamma_\mathrm{in} \\ s_+/2 & \text{on } C_1 \cup C_3 \\ -s_+/2 & \text{on } C_2 \cup C_4 \\ g(y) & \text{on } S_1 \cup S_3 \\ g(x) & \text{on } S_2 \cup S_4; \end{cases} \tag{3.7}$$

and

$$q_3(x,\, y) = q_{3,\mathrm{b}}(x,\, y) := \begin{cases} 0 & \text{on } \Gamma_\mathrm{in} \\ -s_+/6 & \text{on } \Gamma_\mathrm{out}. \end{cases} \tag{3.8}$$

For solutions of the form (3.6), the LdG Euler-Lagrange system (2.12) reduces to

$$\begin{aligned} \Delta q_1 &= \frac{\lambda^2}{L} \left\{ A q_1 + 2B q_1 q_3 + 2C \left(q_1^2 + 3 q_3^2 \right) q_1 \right\}, \\ \Delta q_3 &= \frac{\lambda^2}{L} \left\{ A q_3 + B \left(\frac{1}{3} q_1^2 - q_3^2 \right) + 2C \left(q_1^2 + 3 q_3^2 \right) q_3 \right\}. \end{aligned} \tag{3.9}$$

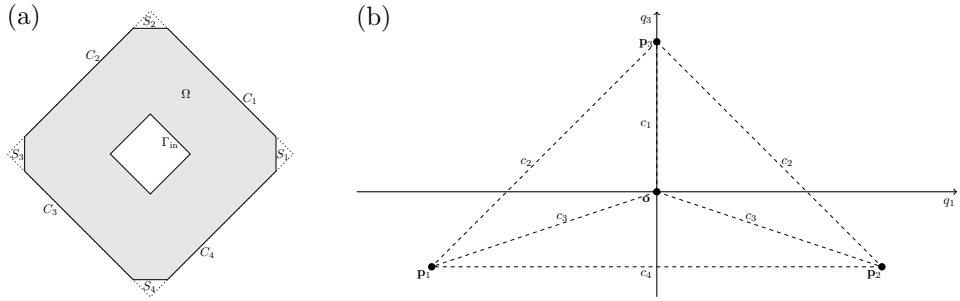

FIGURE 3.1. *(a) The domain Ω. (b) The four critical points of the potential F, which is defined by Eq. (3.11). The dashed lines indicate the "transition costs" that are defined by Eq. (4.3).*

PROPOSITION 3.1. *We have a critical point (q_1^s, q_3^s), of (3.10) in the admissible space (3.5), subject to the boundary conditions (3.7) and (3.8), such that $q_1 = 0$ on $x = 0$ and $y = 0$. This pair defines a LdG critical point of the form (3.6): a Well Order Reconstruction solution "WORS" for a square with an isotropic inclusion.*

Proof. Let

$$J_\lambda[q_1, q_3] := \int_\Omega \left(|\nabla q_1|^2 + 3|\nabla q_3|^2 + \frac{\lambda^2}{L} F(q_1,\, q_3) \right) \mathrm{d}A, \tag{3.10}$$

where F is the polynomial potential given by

$$F(q_1,\, q_3) := A(q_1^2 + 3q_3^2) + 2B\, q_3\, (q_1^2 - 2q_3^2) + C(q_1^2 + 3q_3^2)^2 - F_{\min} \tag{3.11}$$

and $F_{\min} := As_+^2/3 - 2Bs_+^3/27 + Cs_+^4/9$ is a constant chosen so that $\inf F = 0$. F has exactly four critical points in the $(q_1,\, q_3)$-plane: the origin $(0,\, 0)$, which is a local maximum, and the points

$$\mathbf{p}_1 := (-s_+/2,\, -s_+/6), \qquad \mathbf{p}_2 := (s_+/2,\, -s_+/6), \qquad \mathbf{p}_3 := (0,\, s_+/3), \tag{3.12}$$

which are global minima; see Figure 3.1(b). The partial differential equations (3.9) are precisely the Euler-Lagrange equations for J in (3.10).
We follow the ideas in [43] and minimize the functional $J[q_1,\, q_3]$ on a quadrant of the rescaled domain (3.1). On the quadrant, the boundary condition on C_1 is fixed by Equation (3.7), we have $q_1 = q_3 = 0$ on Γ_{in} and we need additional boundary conditions on the square diagonals. We impose $q_1 = 0$ on the diagonals, $x = 0$ and $y = 0$. Further, we impose $\frac{\partial q_3}{\partial x} = 0$ on $x = 0$ and $\frac{\partial q_3}{\partial y} = 0$ on $y = 0$. We can prove the existence of a minimizer (q_1^*, q_3^*) of $J[q_1,\, q_3]$ on the quadrant in $W^{1,2}$, subject to these boundary conditions, from the direct method in the calculus of variations [26]. We define q_1^s on the square by an odd reflection of q_1^* about the square diagonals and q_3^s by an even reflection of q_3^* about the square diagonals. By using the same arguments as in [43], we can check that (q_1^s, q_3^s) is a critical point of $J[q_1,\, q_3]$ (and hence a solution of (3.9)) on the square with an isotropic inclusion, with the property $q_1 = 0$ on $x = 0$ and $y = 0$. This is the WORS by analogy with [4]. ∎

The corresponding WORS-LdG critical point is given by

$$\mathbf{Q}_s = q_1^s(x,\, y)\, (\mathbf{n}_1 \otimes \mathbf{n}_1 - \mathbf{n}_2 \otimes \mathbf{n}_2) + q_3^s(x,\, y)\, (2\hat{\mathbf{z}} \otimes \hat{\mathbf{z}} - \mathbf{n}_1 \otimes \mathbf{n}_1 - \mathbf{n}_2 \otimes \mathbf{n}_2)\,, \tag{3.13}$$

where (q_1^s, q_3^s) is defined in Proposition 3.1. In particular, $\mathbf{Q}_s$ is a solution of the full system in (2.12). In [43], the authors study the WORS on a square domain without

an isotropic inclusion and hence, only have to deal with the outer square edges. At a special temperature, the WORS has constant q_3 in [43] and the WORS-problem reduces to a scalar variational problem. For a square with an isotropic inclusion, the boundary conditions for q_3 on the inner and outer squares do not match and hence, we have inhomogeneous profiles for q_1 and q_3, for all values of A, making this a harder problem. Next, we have a uniqueness result (also see [43] and [14]).

PROPOSITION 3.2. *The WORS in (3.13) is the unique LdG critical point (and hence, globally stable) for either λ sufficiently small or for ρ sufficiently close to 1 i.e. for either very small squares or when the aspect ratio approaches unity.*

Proof. The proof follows by the arguments in Proposition 4.2 of [14], provided we can bound the Poincaré constant of Ω in terms of the geometric parameter ρ. Let $u \in H^1(\Omega)$ be any scalar function such that $u = 0$ on $\partial\Omega$; we extend u out of Ω by zero. We consider the set $K := \{(x, y) \in \Omega \colon x \geq 0,\, y \geq 0,\, \rho < x + y < 1\}$ and define new variables $(s,\, t)$ by

$$x = ts, \qquad y = t(1 - s)$$

for each $(x, y) \in K$. The variables (s, t) vary in the range $s \in (0,\, 1)$, $t \in (\rho,\, 1)$. We compute the integral of $|u|^2$ over K with respect to the coordinates (s, t), and apply the fundamental theorem of calculus in t-direction, using that $u = 0$ for $t = 1$:

$$\begin{aligned} \int_K |u(\mathbf{x})|^2 \,\mathrm{d}\mathbf{x} = \int_0^1 \int_\rho^1 t|u(s,t)|^2 \,\mathrm{d}t\,\mathrm{d}s \leq \int_0^1 \int_\rho^1 t \left| \int_t^1 \partial_\xi u(s,\xi)\,\mathrm{d}\xi \right|^2 \,\mathrm{d}t\,\mathrm{d}s \\ \leq \int_0^1 \int_\rho^1 \int_t^1 t(1-t)\left|\partial_\xi u(s,\xi)\right|^2 \,\mathrm{d}\xi\,\mathrm{d}t\,\mathrm{d}s. \end{aligned} \tag{3.14}$$

The last inequality follows by the Hölder inequality. Now, we have $|\partial_t u|^2 = |s\partial_x u + (1-s)\partial_y u|^2 \leq s|\partial_x u|^2 + (1-s)|\partial_y u|^2 \leq |\nabla u|^2$, where ∇ denotes the gradient with respect to (x, y). Using this with $\rho \leq t \leq \xi$, and reverting to the original coordinates $(x,\, y)$, we obtain

$$\int_K |u(\mathbf{x})|^2 \mathrm{d}\mathbf{x} \leq (1-\rho)^2 \int_0^1 \int_\rho^1 \xi \left|\partial_\xi u(s,\xi)\right|^2 \,\mathrm{d}\xi\,\mathrm{d}s \leq (1-\rho)^2 \int_K |\nabla u(\mathbf{x})|^2 \mathrm{d}\mathbf{x}.$$

We repeat the same argument on the other quadrants and add the resulting inequalities to conclude that

$$\int_\Omega |u(\mathbf{x})|^2 \,\mathrm{d}\mathbf{x} \leq (1-\rho)^2 \int_\Omega |\nabla u(\mathbf{x})|^2 \,\mathrm{d}\mathbf{x}. \tag{3.15}$$

By the maximum principle, as in [27, Proposition 3], any solution $\mathbf{Q}$ of (2.12) in the admissible class (3.5) is bounded, i.e. $|\mathbf{Q}(\mathbf{x})| \leq M$ for any $\mathbf{x} \in \Omega$ where M only depends on the coefficients A, B, C. Now, by repeating verbatim the arguments in [14, Lemma 8.2], and using the Poincaré inequality (3.15), we conclude that the boundary value problem (2.12), (3.2), (3.3), (3.4) has a unique solution for

$$(1-\rho)^2\lambda^2 < \kappa L,$$

where κ is a positive constant that only depends on A, B, C. ∎

4. The limit of large domains. Next, we analyze the asymptotic behavior of minimizers of (3.10) in the $\lambda \to +\infty$ limit. To this end, we introduce some notation. We denote $\mathbf{q} := (q_1, q_3)$ and define a metric d on the $\mathbf{q}$-plane: for any two points $\mathbf{q}_0$, $\mathbf{q}_1 \in \mathbb{R}^2$, we let

(4.1)
$$d(\mathbf{q}_0, \mathbf{q}_1) := \inf \left\{ \int_0^1 F^{1/2}(\mathbf{q}(t)) |\mathbf{q}'(t)| \, \mathrm{d}t \colon \mathbf{q} \in C^1([0, 1]; \mathbb{R}^2),\ \mathbf{q}(0) = \mathbf{q}_0,\ \mathbf{q}(1) = \mathbf{q}_1 \right\}.$$

This is the geodesic distance associated with the Riemannian metric $F^{1/2}$. However, this metric is degenerate, in that $F^{1/2}(\mathbf{p}_1) = F^{1/2}(\mathbf{p}_2) = F^{1/2}(\mathbf{p}_3) = 0$ for $\mathbf{p}_1$, $\mathbf{p}_2$, $\mathbf{p}_3$ given by (3.12). Despite the degeneracy, it can be proven that the infimum in (4.1) is actually achieved by a minimizing geodesic, for any $\mathbf{q}_0$, $\mathbf{q}_1 \in \mathbb{R}^2$ (this follows by the arguments in [29, Lemma 9]).

Let $\mathcal{H}^1(E)$ denote the length of a set $E \subseteq \mathbb{R}^2$ (or, more formally, its 1-dimensional Hausdorff measure). For every measurable subset $E \subseteq \Omega$, let χ_E be the characteristic function of E (i.e., $\chi_E(x) := 1$ for $x \in E$, and $\chi_E(x) := 0$ otherwise) and let $\partial^* E$ be the reduced boundary of E, that is, the set of points $x \in \partial E$ such that the limit

$$\nu_E(x) := \lim_{\rho \searrow 0} \frac{\mathrm{D}\chi_E(B_\rho(x))}{|\mathrm{D}\chi_E|(B_\rho(x))}$$

exists and $|\nu_E(x)| = 1$. (Here $\mathrm{D}\chi_E$ stands for the distributional derivative of χ_E, which is a measure, and $|\mathrm{D}\chi_E|$ is the total variation measure; see, e.g., the book [26].) The reduced boundary is a subset $\partial^* E \subseteq \partial E$ with the following property:

$$\mathcal{H}^1(\partial^* E \cap \Omega) = \sup \left\{ \int_E \operatorname{div} \varphi \, \mathrm{d}A \colon \varphi \in C^1_{\mathrm{c}}(\Omega),\ |\varphi| \le 1 \text{ on } \Omega \right\},$$

(see, e.g., [46, Section 14]). If E has a regular (say, piecewise C^1) boundary, by the Gauss-Green theorem the right-hand side of this formula reduces to $\mathcal{H}^1(\partial E \cap \Omega)$, and indeed $\partial^* E = \partial E$ in this case; however, for a generic set E with non-regular boundary, we might have $\partial^* E \subsetneq \partial E$.

Finally, we set $\mathbf{q}_{\mathrm{b}} := (q_{1,\mathrm{b}}, q_{3,\mathrm{b}})$, where $q_{1,\mathrm{b}}$, $q_{3,\mathrm{b}}$ are defined by (3.7), (3.8) respectively. Let $\mathbf{q}_\lambda := (q_1, q_3)$ be a minimizer of the functional (3.10), for $\lambda > 0$.

PROPOSITION 4.1. *There exists a subsequence $\lambda_j \nearrow +\infty$ such that $\mathbf{q}_{\lambda_j}$ converges, in $L^1(\Omega)$ and a.e., to a map of the form*

$$\mathbf{q}_\infty = \sum_{k=1}^{3} \mathbf{p}_k \, \chi_{E_k^*}.$$

Here $\mathbf{p}_1$, $\mathbf{p}_2$, $\mathbf{p}_3$ are defined by (3.12), and E_1^*, E_2^*, E_3^* are measurable, pairwise disjoint sets such that $\Omega = E_1^* \cup E_2^* \cup E_3^*$. Moreover, E_1^*, E_2^*, E_3^* minimize the following functional:

(4.2)
$$J_\infty[E_1, E_2, E_3] := \sum_{i,j=1}^{3} d(\mathbf{p}_i, \mathbf{p}_j) \, \mathcal{H}^1(\partial^* E_i \cap \partial^* E_j \cap \Omega) + \int_{\partial\Omega} d(\mathbf{q}_\infty(\mathbf{r}), \mathbf{q}_{\mathrm{b}}(\mathbf{r})) \, \mathrm{d}\mathcal{H}^1(\mathbf{r})$$

among all possible choices of measurable, pairwise disjoint sets E_1, E_2, E_3 such that $\Omega = E_1 \cup E_2 \cup E_3$.

The sets E_1^*, E_2^*, E_3^* give an optimal partition of the domain Ω, in the sense that they minimise the functional (4.2). This functional depends on the length of the transition layers $\partial^* E_i \cap \partial^* E_j$ and on $d(\mathbf{p}_i, \mathbf{p}_j)$, which is the energy cost of a transition from $\mathbf{p}_i$ to $\mathbf{p}_j$. The functional (3.10) also has a boundary term, which accounts for the possible presence of boundary layers.

Proof of Proposition 4.1. This result can be shown using classical arguments in the theory of Γ-convergence. More precisely, Proposition 4.1 follows by the main result in [38] (see also [39, Theorem 3.9] or [30, Theorem 7.20] for similar results). The analysis in [38, 39] does not take into account the presence of boundary conditions, such as (3.7)–(3.8). However, these can be included by straightforward modifications of the arguments, as indicated in [30, Section 4.2.1 and Theorem 7.10]. ∎

Let us introduce the transition costs

$$
\begin{aligned}
&c_1 := d(\mathbf{o}, \mathbf{p}_3), && c_2 := d(\mathbf{o}, \mathbf{p}_1) = d(\mathbf{o}, \mathbf{p}_2),\\
&c_3 := d(\mathbf{p}_1, \mathbf{p}_3) = d(\mathbf{p}_2, \mathbf{p}_3), && c_4 := d(\mathbf{p}_1, \mathbf{p}_2),
\end{aligned}
\tag{4.3}
$$

where $\mathbf{o} := (0, 0)$ is the origin in the (q_1, q_3)-plane and d is the intrinsic distance defined by (4.1). These costs c_1, c_2, c_3, c_4 are functions of A, B, C. We have used the symmetry of the function F, in (3.11), to deduce that $d(\mathbf{o}, \mathbf{p}_1) = d(\mathbf{o}, \mathbf{p}_2)$ and $d(\mathbf{p}_3, \mathbf{p}_1) = d(\mathbf{p}_3, \mathbf{p}_2)$. By analyzing the possible configurations of (E_1, E_2, E_3), we can identify three candidate minimizers for (4.2) and compute their energies in terms of the c_i in (4.3). For the sake of simplicity, we assume that $\varepsilon = 0$ in what follows, i.e. an un-truncated domain Ω. This is acceptable because, when ε is small, the contribution of the truncated edges to the boundary integral in (4.2) is negligible.

- A configuration with $\mathbf{q} = \mathbf{p}_1$ on the first and third quadrant, and $\mathbf{q} = \mathbf{p}_2$ on the second and fourth quadrant (i.e., $E_1 = \{(x, y) \in \Omega \colon xy \geq 0\}$, $E_2 = \{(x, y) \in \Omega \colon xy < 0\}$, $E_3 = \emptyset$). This is the *the $\lambda \to +\infty$ limit of the WORS*. It has transition layers from the isotropic state to $\mathbf{p}_1$ or $\mathbf{p}_2$ over Γ_1, and transition layers $\mathbf{p}_1 \to \mathbf{p}_2$ on the diagonals. Using (4.2), the energy of this WORS-like configuration is

$$
J_\infty(\mathrm{WORS}) = 4\sqrt{2}\rho c_2 + 4\,(1-\rho)\,c_4.
$$

- Two configurations related by symmetry, with $\mathbf{q} = \mathbf{p}_1$, respectively $\mathbf{q} = \mathbf{p}_2$ over almost the entire domain, Ω. Equivalently, in terms of the E_k, these configurations are defined by $E_1 = \Omega$, $E_2 = E_3 = \emptyset$ and $E_2 = \Omega$, $E_1 = E_3 = \emptyset$, respectively. These configurations have a transition layer at the inner boundary, from the isotropic to a uniaxial state (either $\mathbf{p}_1$ or $\mathbf{p}_2$), and two *boundary layers* on the edges C_2, C_4 respectively (or C_1, C_3), to account for the boundary conditions (3.7)–(3.8). We refer to these states as *BD* states, to abbreviate for boundary distortion, since they have two distinctive transition layers along a pair of parallel outer edges. These two BD configurations are energetically degenerate with energy

$$
J_\infty(\mathrm{BD}) = 4\sqrt{2}\,\rho c_2 + 2\sqrt{2} c_4.
$$

- A configuration with $\mathbf{q} = \mathbf{p}_3$ in a neighbourhood of the inner boundary, surrounded by the same cross structure as in the WORS, that is,

$$
\begin{aligned}
&E_3 = \{(x, y) \in \Omega \colon |x + y| \leq \rho + \eta,\ |x - y| \leq \rho + \eta\},\\
&E_1 = \{(x, y) \in \Omega \setminus E_3 \colon xy \geq 0\},\\
&E_2 = \{(x, y) \in \Omega \setminus E_3 \colon xy < 0\}.
\end{aligned}
\tag{4.4}
$$

In this *"escaped"* configuration (ESC), the isotropic inclusion is surrounded by a uniaxial region, E_3, with positive order parameter or equivalently $q_3 > 0$. This may be energetically convenient, if the transition $\mathbf{p}_1 \to \mathbf{p}_2$ is energetically very expensive, compared to the transitions $\mathbf{o} \to \mathbf{p}_3$ and $\mathbf{p}_3 \to \mathbf{p}_1$, $\mathbf{p}_3 \to \mathbf{p}_2$. If this is the case, the escaped configuration reduces the length of the (very expensive) transition layer along the diagonals, at the price of introducing a new transition layer near the core. The overall cost is given by

$$J_\infty(\text{ESC}) = 4\sqrt{2}\rho c_1 + 4\sqrt{2}\,(\rho+\eta)\,c_3 + 4\,(1-\rho-\eta)\,c_4.$$

A configuration with an island of $\mathbf{p}_3$ around the core, surrounded by a constant state $\mathbf{p}_1$ or $\mathbf{p}_2$, always has greater energy than the competing BD-configuration. This follows from the triangle inequality for the metric d, which gives $c_1 + c_3 \geq c_2$. Other configurations, that have "two-steps transition layers", e.g. a transition of the form $\mathbf{p}_1 \to \mathbf{p}_3 \to \mathbf{p}_2$ occurring along the diagonals, are energetically more expensive than the WORS, BD and the ESC configurations . Configurations with non-straight transition layers can also be ruled out, since they have greater energetic costs than straight transition layers. We do not consider these configurations with higher energies here. Now, we can compare the energies of the WORS, BD and ESC configurations in this limit of large domains.

- $J_\infty(\text{WORS}) < J_\infty(\text{BD})$ if and only if $\rho > 1 - \sqrt{2}/2$.
- We compare $J_\infty(\text{ESC})$ with $J_\infty(\text{WORS})$. By substituting the explicit expressions for the two energies, we see that $J_\infty(\text{ESC}) < J_\infty(\text{WORS})$ implies

  $$(\sqrt{2}c_3 - c_4)\eta < \sqrt{2}(c_2 - c_1 - c_3)\rho,$$

  and the right-hand side is always non-positive, due to the triangle inequality. Thus, for this inequality to hold, we must have $c_4 > \sqrt{2}c_3$. By imposing the geometric constraint $\eta \leq 1 - \rho$, we obtain

  $$\frac{\sqrt{2}(c_1 - c_2 + c_3)}{(c_4 - \sqrt{2}c_3)}\rho \leq 1 - \rho.$$

  By straightforward algebraic manipulations, we conclude that $J_\infty(\text{ESC}) < J_\infty(\text{WORS})$ holds if and only if

  $$\begin{cases} c_4 > \sqrt{2}c_3 \\ 0 < \rho < R_1, \end{cases} \quad \text{or} \quad \begin{cases} c_4 > \sqrt{2}c_3 \\ R_1 < 0, \end{cases}$$

  where

  $$R_1 := \frac{c_4 - \sqrt{2}c_3}{\sqrt{2}c_1 - \sqrt{2}c_2 + c_4}.$$

- Arguing similarly, we conclude that $J_\infty(\text{ESC}) < J_\infty(\text{BD})$ if and only if

  $$\begin{cases} c_4 > \sqrt{2}c_3 \\ c_2 > c_1 \\ R_2 < \rho < 1 \end{cases} \quad \text{or} \quad \begin{cases} c_4 > \sqrt{2}c_3 \\ c_1 > c_2 \\ 0 < \rho < R_2, \end{cases}$$

  where

  $$R_2 := \frac{c_4 - 2c_3}{2c_1 - 2c_2}.$$

5. Numerics. Let $\bar{\lambda}^2 = \dfrac{2C\lambda^2}{L}$, and we take

$$B = 0.64 \times 10^4 \mathrm{Nm}^{-2}, \quad C = 0.35 \times 10^4 \mathrm{Nm}^{-2}, \quad A = -\frac{B^2}{3C}, \quad \bar{\lambda}^2 = 200 \tag{5.1}$$

throughout this section if not stated differently. We choose this special value of A because in the absence of a square inclusion, the WORS has a particularly simple parametrization in terms of a single variable q_1 and constant q_3 (see (3.6)) at this temperature [43]. In fact, this is the only temperature for which the system (3.9) has a solution with constant q_3. Of course, we cannot have solutions with constant q_3 for this model problem because of the inhomogeneous boundary conditions but we still regard $A = -\frac{B^2}{3C}$ as a reference point for easy comparison with the results in [43]. We assume that $\bar{\lambda}^2 = 200$ is large enough for the asymptotic estimates in Section 4 to hold; we have checked the trends with larger values of $\bar{\lambda}^2$ and they are qualitatively the same.

5.1. Transition Costs. First, we compute the c_i in (4.3). According to standard arguments in Riemannian geometry (see e.g. [47, Chapter 3]), the intrinsic distance $d(\mathbf{q}_0, \mathbf{q}_1)$, i.e. geodesic distance, defined in (4.1) can be calculated alternatively as

$$d(\mathbf{q}_0, \mathbf{q}_1) = \inf\left\{ \left(\int_0^1 F(\mathbf{q}(t)) |\mathbf{q}'(t)|^2 \, \mathrm{d}t \right)^{1/2} : \mathbf{q} \in C^1([0,1]; \mathbb{R}^2),\ \mathbf{q}(0) = \mathbf{q}_0,\ \mathbf{q}(1) = \mathbf{q}_1 \right\}.$$

The profiles of the geodesic, $\mathbf{q}(t) = (q_1(t), q_3(t))$, in each case of (4.3) are shown in Fig. 5.1; these are the optimal profiles which minimise the intrinsic distance between the four critical points $\mathbf{o}, \mathbf{p}_1, \mathbf{p}_2, \mathbf{p}_3$ and the associated costs are:

$$c_1 = 22.3067, \quad c_2 = 34.7378, \quad c_3 = 41.6817, \quad c_4 = 60.2955. \tag{5.2}$$

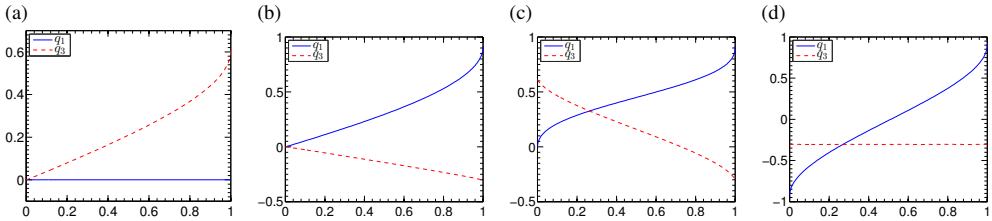

FIGURE 5.1. *The profiles of the geodesic,* $\mathbf{q}(t) = (q_1(t), q_3(t))$*, for different* $\mathbf{q}_0$ *and* $\mathbf{q}_1$ *(*$A = -\frac{B^2}{3C}$*).*

Hence,

$$c_2 > c_1, \quad c_4 > \sqrt{2} c_3, \quad R_2 > R_1. \tag{5.3}$$

In view of the discussion in the previous section,

$$\min\{J_\infty(\mathrm{WORS}),\ J_\infty(\mathrm{BD})\} < J_\infty(\mathrm{ESC})$$

requires that

$$R_2 < \rho < R_1, \quad \text{if } c_4 > \sqrt{2} c_3 \text{ and } c_2 > c_1, \tag{5.4}$$

which cannot hold since $R_2 > R_1$. Therefore, ESC cannot be energetically preferred to either the WORS or BD for this choice of parameters.
We also perform a systematic search of the parameter space in terms of A, for fixed B and C; the transition costs c_i and the quantities R_i, are numerically computed and plotted in Fig. 5.2, as a function of the reduced temperature $t = \frac{27AC}{B^2}$. We note that $c_2 > c_1$ and $R_2 > R_1$ hold true in all the numerical simulations. Hence, the ESC cannot be energetically preferred to either the WORS or BD if $c_4 < \sqrt{2}c_3$ or if $c_4 > \sqrt{2}c_3$ and $R_2 > R_1$ (by the same arguments as above), according to the estimates in the previous section.

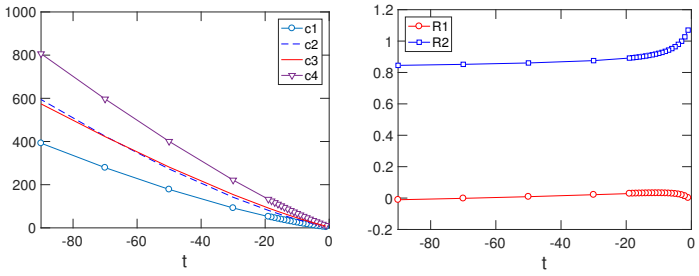

FIGURE 5.2. *The value of c_i and R_i as a function of $t = \frac{27AC}{B^2}$.*

5.2. WORS and BD on a square with an isotropic inclusion. For the following simulations, we take

$$\Omega = \{(x, y) \in \mathbb{R}^2 \colon \rho < \max\{|x|, |y|\} < 1\}, \tag{5.5}$$

as the domain and seek numerical solutions of the form

$$\mathbf{Q}(x, y) = q_1(x, y)(\mathbf{e}_x \otimes \mathbf{e}_x - \mathbf{e}_y \otimes \mathbf{e}_y) + q_3(x, y)(2\mathbf{e}_z \otimes \mathbf{e}_z - \mathbf{e}_x \otimes \mathbf{e}_x - \mathbf{e}_y \otimes \mathbf{e}_y), \tag{5.6}$$

where $\mathbf{e}_x$, $\mathbf{e}_y$ and $\mathbf{e}_z$ are unit-vectors in the x-, y- and z-directions respectively, subject to the boundary conditions

$$\begin{aligned} &\mathbf{Q}(x, y) = 0, \qquad \text{on } \Gamma_{\text{in}}, \\ &\mathbf{Q}(x, \pm 1) = \frac{s_+}{2}(\mathbf{e}_x \otimes \mathbf{e}_x - \mathbf{e}_y \otimes \mathbf{e}_y) - \frac{s_+}{6}(2\mathbf{e}_z \otimes \mathbf{e}_z - \mathbf{e}_x \otimes \mathbf{e}_x - \mathbf{e}_y \otimes \mathbf{e}_y), \\ &\mathbf{Q}(\pm 1, y) = -\frac{s_+}{2}(\mathbf{e}_x \otimes \mathbf{e}_x - \mathbf{e}_y \otimes \mathbf{e}_y) - \frac{s_+}{6}(2\mathbf{e}_z \otimes \mathbf{e}_z - \mathbf{e}_x \otimes \mathbf{e}_x - \mathbf{e}_y \otimes \mathbf{e}_y). \end{aligned} \tag{5.7}$$

As shown in Section 2, for LdG critical points of the form (5.6) with two degrees of freedom, the Euler-Lagrange equations (2.12) reduce to

$$\begin{cases} \Delta q_1 = \bar{\lambda}^2 \left(\dfrac{A}{2C} q_1 + \dfrac{B}{C} q_1 q_3 + (q_1^2 + 3q_3^2) q_1 \right) \\ \Delta q_3 = \bar{\lambda}^2 \left(\dfrac{A}{2C} q_3 + \dfrac{B}{C} (\frac{1}{3} q_1^2 - q_3^2) + (q_1^2 + 3q_3^2) q_3 \right). \end{cases} \tag{5.8}$$

We use a standard finite-difference method five-point formula for Δ) [40] and Newton's Method to solve the system (5.8). We plot q_1, q_3 and the biaxiality parameter

$$\beta^2 = 1 - 6 \frac{\left(\text{tr}(\mathbf{Q}^3)\right)^2}{\left(\text{tr}(\mathbf{Q}^2)\right)^3}$$

for the WORS and BD, for $\bar{\lambda}^2 = 200$ and $\rho = 0.2$ in Fig. 5.3. The biaxiality parameter $\beta^2 \in [0, 1]$ for $\{\mathbf{Q} \neq \mathbf{0}\}$, β^2 vanishes when $\mathbf{Q}$ is uniaxial and β^2 is unity when one of the eigenvalues vanishes and the corresponding $\mathbf{Q}$ is maximally biaxial [43]. The

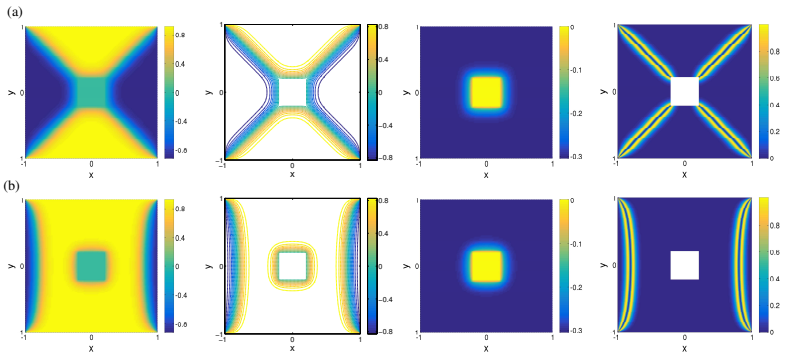

FIGURE 5.3. *(a) The WORS for $\bar{\lambda}^2 = 200$ and $\rho = 0.2$. Left to right: plot and contour plot of q_1, plot of q_3, and plot of biaxiality parameter β^2. (b)A BD-solution for $\bar{\lambda}^2 = 200$ and $\rho = 0.2$. Left to right: plot and contour plot of q_1, plot of q_3, and plot of biaxiality parameter β^2.*

WORS has a uniaxial cross with negative order parameter, connecting the vertices of the inner and the outer squares. The BD solution is distinguished by a pair of transition layers, localized near $x = \pm 1$ (or $y = \pm 1$), with $q_1 = 0$. In both cases, q_3 decreases monotonically from zero on Γ_{in} to $q_3 = -\frac{B}{6C}$ on the outer boundary.

We compare free energies of BD and the WORS for $\bar{\lambda}^2 = 200$ and various ρ in Fig. 5.4(a), which shows that the WORS is energetically preferred for relatively large ρ. Indeed, the Γ-convergence argument in the previous section shows that, in the limit $\bar{\lambda}^2 \to \infty$, we have $J_\infty(\text{WORS}) < J_\infty(\text{BD})$ if and only if $\rho > 1 - \sqrt{2}/2$. Numerically, we compute the critical value $\rho_0(\bar{\lambda}^2)$, such that $J_{\bar{\lambda}^2}(\text{BD}) = J_{\bar{\lambda}^2}(\text{WORS})$ when $\rho = \rho_0(\bar{\lambda}^2)$, as a function of $\bar{\lambda}^2$ in Fig. 5.4(b). Qualitatively, we see that $\rho_0(\bar{\lambda}^2) \to 1 - \sqrt{2}/2$ when $\bar{\lambda}^2 \to \infty$, as expected.

Since the WORS is the unique LdG critical point for either λ sufficiently small or for ρ sufficiently close to 1, BD-solutions cannot be critical points of (3.10) in these regimes. Numerically, we find that for each $\bar{\lambda}^2$, there exists a critical value $\rho_1(\bar{\lambda}^2)$, for which BD-solutions are no longer critical points of (3.10) when $\rho \geq \rho_1(\bar{\lambda}^2)$. This critical value $\rho_1(\bar{\lambda}^2)$ is found by increasing ρ gradually till we cannot numerically obtain a BD slution with a BD-like initial guess, even with the deflation technique [41]. For $\bar{\lambda}^2 = 100$, $\rho_1 \approx 0.28$, whilst for the $\bar{\lambda}^2 = 200$, $\rho_1 \approx 0.42$. We plot $\rho_1(\bar{\lambda}^2)$ as a function of $\bar{\lambda}^2$ in Fig. 5.4(c). By adapting arguments in [14] to a truncated square annulus such as ours (see also the proof of Proposition 3.2), we can show that the LdG energy (2.1) is strictly convex for

$$1 - C_1 \bar{\lambda}^{-1} < \rho < 1,$$

where C_1 is a positive constant independent of ρ and $\bar{\lambda}^2$. In this range, WORS is the unique critical point and this range becomes narrower as $\bar{\lambda}$ increases.

The stabilities of the WORS and BD can be tested by solving the gradient flow

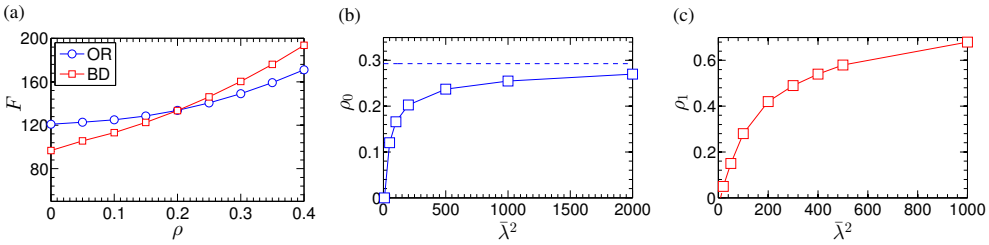

FIGURE 5.4. *(a) Free energies of the* WORS *and* BD *for various* ρ *at* $\bar{\lambda}^2 = 200$. *(b) Critical value* ρ_0, *for which* $J_{\bar{\lambda}^2}(\text{BD}) = J_{\bar{\lambda}^2}(\text{WORS})$; *the limiting value,* $1-\sqrt{2}/2$, *is shown by the dash line. (c) Critical value* $\rho_1(\bar{\lambda}^2)$, *for which BD is no longer a critical point of* (3.10) *when* $\rho \geq \rho_1(\bar{\lambda}^2)$.

equations for q_1 and q_3 in Ω as shown below:

$$\begin{cases} \partial_t q_1 = \Delta q_1 - \bar{\lambda}^2 \left(\dfrac{A}{2C} q_1 + \dfrac{B}{C} q_1 q_3 + (q_1^2 + 3q_3^2) q_1 \right) \\ \partial_t q_3 = \Delta q_3 - \bar{\lambda}^2 \left(\dfrac{A}{2C} q_3 + \dfrac{B}{C} (\dfrac{1}{3} q_1^2 - q_3^2) + (q_1^2 + 3q_3^2) q_3 \right), \end{cases} \tag{5.9}$$

for $\bar{\lambda}^2 = 200$, subject to the Dirichlet boundary conditions (3.2), (3.3) and (3.4) and different initial conditions. We use a standard five-point finite-difference scheme for Δ and the Crank-Nicolson scheme [40] for time-stepping in the numerical simulations.

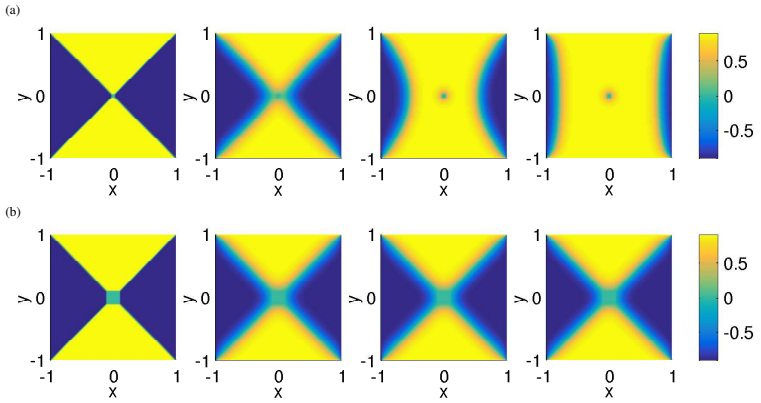

FIGURE 5.5. *(a) The profiles of* q_1 *for* $t = 0$, $t = 0.2$, $t = 0.5$ *and* $t = 2(\rho = 0.02,\ \bar{\lambda}^2 = 200)$. *(b) The profiles of* q_1 *for* $t = 0$, $t = 0.2$, $t = 0.5$ *and* $t = 2(\rho = 0.1,\ \bar{\lambda}^2 = 200)$.

In Fig. 5.5, we solve (5.9) with a WORS-like initial condition as described below

$$q_1(x,y) = \begin{cases} s_+/2 & \text{for } -|y| < x < |y| \\ -s_+/2 & \text{for } -|x| < y < |x|, \end{cases} \qquad q_3(x,y) = -s_+/6, \quad \forall (x,y) \in \Omega \tag{5.10}$$

for $\bar{\lambda}^2 = 200$ with $\rho = 0.02$ and $\rho = 0.1$, respectively. The dynamic evolutions of q_1 are shown in Fig. 5.5. In both cases, ρ is such that $J(\text{WORS}) > J(\text{BD})$ according to Fig. 5.4(a) and yet the evolutions are different. For $\rho = 0.02$, the WORS-like initial condition evolves to a BD solution and for $\rho = 0.1$, the WORS-like initial condition converges to the WORS, which indicates that the WORS is metastable for $\rho = 0.1$, with a basin of attraction. We also solve (5.9) with a BD-like initial condition for

$\bar{\lambda}^2 = 200$, with $\rho = 0.4$ and $\rho = 0.44$. The previous discussions illustrate that BD-solutions are not critical points of (3.10) for $\rho \gtrsim 0.42$. We choose two values of ρ that are at either end of this critical value. For $\rho = 0.44$, the solution converges to the WORS as expected. For $\rho = 0.4$, the numerical solution converges to a BD-solution, although BD-solutions have higher free energy than the WORS, illustrating that BD-solutions remain metastable for a range of $\rho \in \left(0, \rho_1(\bar{\lambda}^2)\right)$.

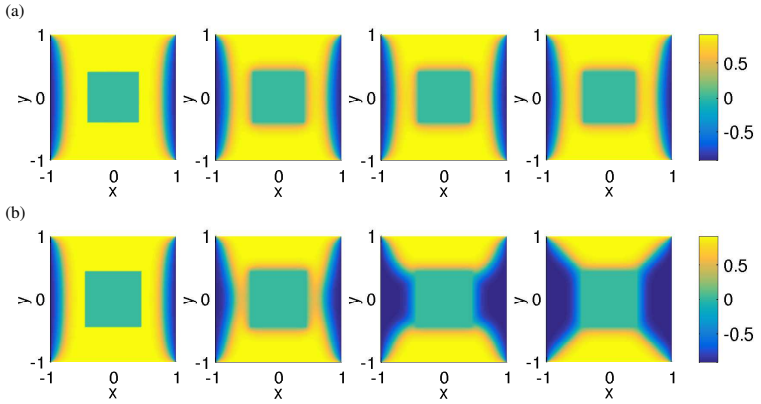

FIGURE 5.6. *(a) The profiles of q_1 for $t = 0$, $t = 0.3$, $t = 0.4$ and $t = 2$ ($\rho = 0.4$, $\bar{\lambda}^2 = 200$). (b) The profiles of q_1 for $t = 0$, $t = 0.3$, $t = 0.4$ and $t = 2$ ($\rho = 0.44$, $\bar{\lambda}^2 = 200$).*

5.3. Decomposition of the Second Variation of the LdG energy. The gradient flow simulations give us information about the stabilities of the WORS and BD-solutions in the restricted class of $\mathbf{Q}$-tensors that have the form (5.6). In the following, we consider the second variation of the LdG energy (2.10) about the WORS and BD-solutions, for arbitrary perturbations with five degrees of freedom. As is standard in the calculus of variations, a critical point is locally stable if the second variation of the LdG energy is positive for all admissible perturbations and is unstable if there exists a perturbation for which the second variation is negative. Consider $\mathbf{W} = \mathbf{Q} + \epsilon\mathbf{V}$, where $\mathbf{Q}$ is either the WORS or BD-solutions and the perturbation, $\mathbf{V}$, vanishes at the boundary. The second variation of the LdG energy is:

(5.11)
$$\delta^2 F(\mathbf{V}) = \int_\Omega \frac{\lambda^2}{L}\left(A|\mathbf{V}|^2 - 2BQ_{ij}V_{jk}V_{ki} + C|\mathbf{Q}|^2|\mathbf{V}|^2 + 2C(\mathbf{Q}\cdot\mathbf{V})^2\right) + |\nabla\mathbf{V}|^2 \mathrm{d}\mathbf{x}.$$

We write $\mathbf{V}$ as (see [43])

(5.12)
$$\begin{aligned}\mathbf{V}(x,y) &= v_1(x,y)(\mathbf{e}_x\otimes\mathbf{e}_x - \mathbf{e}_y\otimes\mathbf{e}_y) + v_2(x,y)(\mathbf{e}_x\otimes\mathbf{e}_y + \mathbf{e}_y\otimes\mathbf{e}_x)\\ &+ v_3(x,y)(2\mathbf{e}_z\otimes\mathbf{e}_z - \mathbf{e}_x\otimes\mathbf{e}_x - \mathbf{e}_y\otimes\mathbf{e}_y)\\ &+ v_4(x,y)(\mathbf{e}_x\otimes\mathbf{e}_z + \mathbf{e}_z\otimes\mathbf{e}_x) + v_5(x,y)(\mathbf{e}_y\otimes\mathbf{e}_z + \mathbf{e}_z\otimes\mathbf{e}_y),\end{aligned}$$

where we treat the functions, $v_1, \ldots, v_5 \in C_c^\infty(\Omega)$, as perturbations in the five independent basis directions. For LdG critical points with $q_2 = q_4 = q_5 = 0$, such as the

WORS and BD-solutions with constant eigenframes, we have

(5.13)
$$\begin{aligned}\delta^2 F(\mathbf{V}) = \int_\Omega \bar{\lambda}^2 \Bigg(& \frac{A}{C}(v_1^2 + v_2^2 + 3v_3^2 + v_4^2 + v_5^2) \\ & - \frac{B}{C}\big(q_1(v_4^2 - v_5^2) - 2q_3(v_1^2 + v_2^2) + 6q_3 v_3^2 + q_3(v_4^2 + v_5^2) - 4q_1 v_1 v_3\big) \\ & + 2\left(q_1^2 + 3q_3^2\right)(v_1^2 + v_2^2 + 3v_3^2 + v_4^2 + v_5^2) + 4(q_1 v_1 + 3q_3 v_3)^2 \Bigg) \\ & + \left(2|\nabla v_1|^2 + 2|\nabla v_2|^2 + 6|\nabla v_3|^2 + 2|\nabla v_4|^2 + 2|\nabla v_5|^2\right) \mathrm{d}\mathbf{x},\end{aligned}$$

which can be written as

$$\delta^2 F(\mathbf{V}) = \delta^2 F(v_1, v_3) + \delta^2 F(v_2) + \delta^2 F(v_4) + \delta^2 F(v_5), \tag{5.14}$$

where

(5.15)
$$\begin{aligned}\delta^2 F(v_1, v_3) = \int_\Omega \bar{\lambda}^2 \Bigg(& \left(\frac{A}{C} + \frac{2B}{C} q_3 + 6(q_1^2 + q_3^2)\right) v_1^2 + \left(\frac{3A}{C} - \frac{6B}{C} q_3 + 6q_1^2 + 54 q_3^2\right) v_3^2 \\ & + \left(\frac{4B}{C} q_1 + 24 q_1 q_3\right) v_1 v_3 \Bigg) + \left(2|\nabla v_1|^2 + 6|\nabla v_3|^2\right) \mathrm{d}\mathbf{x}, \\ \delta^2 F(v_2) = \int_\Omega \bar{\lambda}^2 & \left(\frac{A}{C} + \frac{2B}{C} q_3 + 2\left(q_1^2 + 3q_3^2\right)\right) v_2^2 + 2|\nabla v_2|^2 \mathrm{d}\mathbf{x}, \\ \delta^2 F(v_4) = \int_\Omega \bar{\lambda}^2 & \left(\frac{A}{C} - \frac{B}{C}(q_1 + q_3) + 2\left(q_1^2 + 3q_3^2\right)\right) v_4^2 + 2|\nabla v_4|^2 \mathrm{d}\mathbf{x}, \\ \delta^2 F(v_5) = \int_\Omega \bar{\lambda}^2 & \left(\frac{A}{C} - \frac{B}{C}(q_3 - q_1) + 2\left(q_1^2 + 3q_3^2\right)\right) v_5^2 + 2|\nabla v_5|^2 \mathrm{d}\mathbf{x}.\end{aligned}$$

Define the subspaces of S_0

$$\begin{aligned}&\mathcal{V}_{13} = \left\{v_1\left(\mathbf{e}_x \otimes \mathbf{e}_x - \mathbf{e}_y \otimes \mathbf{e}_y\right) + v_3\left(2\mathbf{e}_z \otimes \mathbf{e}_z - \mathbf{e}_x \otimes \mathbf{e}_x - \mathbf{e}_y \otimes \mathbf{e}_y\right)\right\}, \\ &\mathcal{V}_2 = \left\{v_2\left(\mathbf{e}_x \otimes \mathbf{e}_y + \mathbf{e}_y \otimes \mathbf{e}_x\right)\right\}, \\ &\mathcal{V}_4 = \left\{v_4\left(\mathbf{e}_x \otimes \mathbf{e}_z + \mathbf{e}_z \otimes \mathbf{e}_x\right)\right\}, \quad \mathcal{V}_5 = \left\{v_5\left(\mathbf{e}_y \otimes \mathbf{e}_z + \mathbf{e}_z \otimes \mathbf{e}_y\right)\right\}.\end{aligned}$$

We can consider perturbations in each subspace respectively. The perturbations in $\mathcal{V}_{13}$ preserve the constant eigenframes of the WORS or BD, the perturbations in $\mathcal{V}_2$ are in-plane perturbations in the (x, y)-plane and preserve the fixed eigenvector $\mathbf{e}_z$, the perturbations in $\mathcal{V}_4$ and $\mathcal{V}_5$ are out-of-plane perturbations such that $\mathbf{W}$ does not have $\mathbf{e}_z$ has a fixed eigenvector for $v_4, v_5 \neq 0$.

Firstly, we consider $\delta^2 F(v_1, v_3)$, which can be regarded as a functional of v_1 and v_3, for given q_1 and q_3. We can minimize $\delta^2 F(v_1, v_3)$ by solving the gradient flow equations

$$\begin{cases}\dfrac{\partial v_1}{\partial t} = \Delta v_1 - \bar{\lambda}^2\left(\dfrac{1}{2} C_{11}(x, y) v_1 + \dfrac{1}{4} C_{13}(x, y) v_3\right) \\ \dfrac{\partial v_3}{\partial t} = \Delta v_3 - \bar{\lambda}^2\left(\dfrac{1}{24} C_{13}(x, y) v_1 + \dfrac{1}{12} C_{33}(x, y) v_3\right),\end{cases} \tag{5.16}$$

with random initial data, where

$$C_{11}(x,y) = \frac{A}{C} + \frac{2B}{C}q_3 + 6q_1^2 + 6q_3^2, \quad C_{13}(x,y) = \frac{4B}{C}q_1 + 24q_1q_3, \tag{5.17}$$
$$C_{33}(x,y) = \frac{3A}{C} - \frac{6B}{C}q_3 + 6q_1^2 + 54q_3^2.$$

For $\bar{\lambda}^2 = 200$, the WORS is a critical point for $0 \leq \rho < 1$, but is unstable for small-ρ. In Fig. 5.7(a), we plot $C_{11}(x,y), C_{13}(x,y)$ and $C_{33}(x,y)$ for the WORS, with $\rho = 0.02$ for which the WORS is unstable. It is relatively straightforward to find v_1 and v_3 such that $\delta F(v_1, v_3) < 0$. An example is shown in Fig. 5.7(b). As expected, the

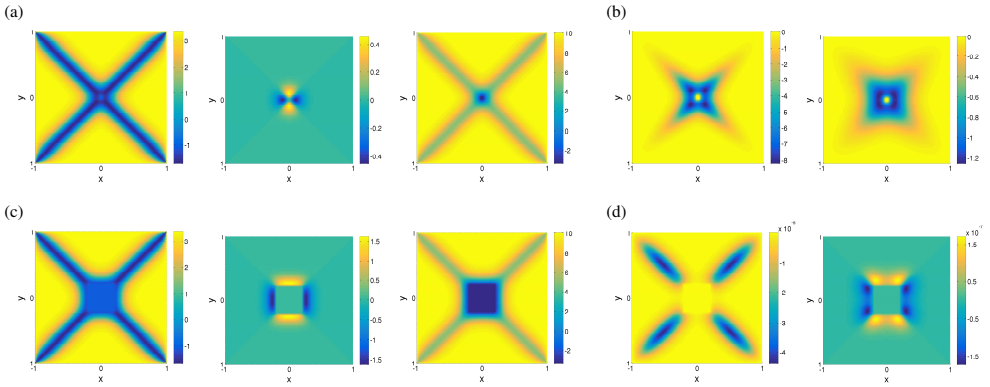

FIGURE 5.7. *(a) The profiles of $C_{11}(x,y)$, $C_{13}(x,y)$ and $C_{33}(x,y)$ for the WORS with $\rho = 0.02$. (b) The profiles of v_1 and v_3 in a perturbation s.t. $\delta^2 F(v_1, v_3) < 0$ for the WORS with $\rho = 0.02$. (c) The profiles of $C_{11}(x,y)$, $C_{13}(x,y)$ and $C_{33}(x,y)$ for the WORS with $\rho = 0.2$. (d) The profiles of v_1 and v_3 in numerical solution of (5.16) for the WORS with $\rho = 0.2$.*

instabilities are localised near the diagonals, they have $v_1 \neq 0$ on the diagonals so that the perturbed WORS loses the diagonal cross to render $\delta^2 F(v_1, v_3) < 0$.

Next we consider the WORS with $\rho = 0.2$. We solve the the gradient flow equations (5.16) with random initial data and the numerical solutions of (5.16), shown in Fig. 5.7(d), converge to $v_1 = v_3 = 0$. This indicates that $\delta^2 F(v_1, v_3) \geq 0$. We find that $\delta^2 F(v_1, v_3) \geq 0$ for the WORS with $\rho \geq 0.05$ and $\bar{\lambda}^2 = 200$. This is consistent with the numerical simulations in [42] and [43] which suggest that the WORS loses stability with respect to BD-solutions in the restricted class of **Q**-tensors (5.6), as either $\bar{\lambda}^2$ increases or ρ decreases.

Similarly, we consider $\delta^2 F(v_1, v_3)$ for BD-solutions, for small-ρ. The numerically computed profiles of $C_{11}(x,y), C_{13}(x,y)$ and $C_{33}(x,y)$ for BD-solutions, with $\rho = 0.02$ and $\rho = 0.2$, are shown in Fig. 5.8. In both cases, the numerical solutions of (5.16), see Fig. 5.8, converge to $v_1 = v_3 = 0$. Our numerical simulations suggest that $\delta^2 F(v_1, v_3) \geq 0$ for BD-solutions for $\rho \geq \rho_1\left(\bar{\lambda}^2\right)$. However, this is not a reflection on the stability of BD with respect to arbitrary perturbations.

Next, we consider $\delta^2 F(v_2)$, which can be minimized by solving the gradient flow equations for v_2

$$\frac{\partial v_2}{\partial t} = 2\Delta v_2 - \bar{\lambda}^2 C_2(x,y) v_2, \tag{5.18}$$

with random initial data, where

$$C_2(x,y) = \frac{A}{C} + \frac{2B}{C}q_3 + 2(q_1^2 + 3q_3^2). \tag{5.19}$$

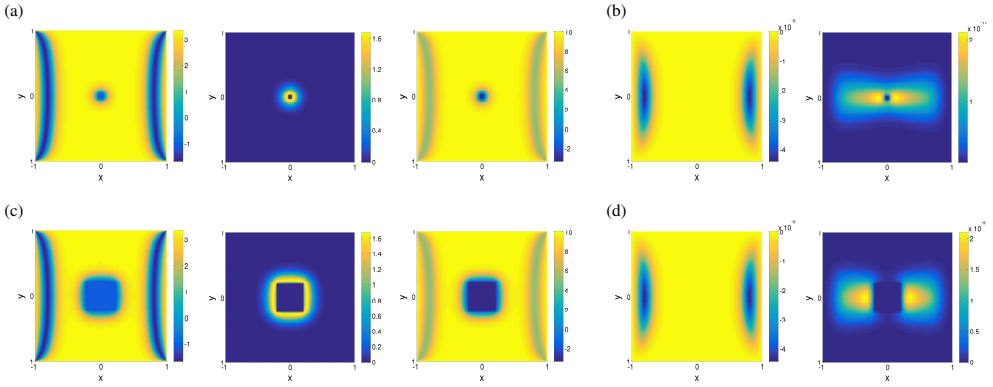

FIGURE 5.8. *(a) The profiles of $C_{11}(x,y)$, $C_{13}(x,y)$ and $C_{33}(x,y)$ for a BD with $\rho = 0.02$. (b) The profiles of v_1 and v_3 in numerical solution of (5.16) for a BD with $\rho = 0.02$. (c) The profiles of $C_{11}(x,y)$, $C_{13}(x,y)$ and $C_{33}(x,y)$ for a BD with $\rho = 0.2$. (d) The profiles of v_1 and v_3 in numerical solution of (5.16) for a BD with $\rho = 0.2$.*

According to our numerical results, $C_2 \leq 0$ for both the WORS and BD, for all ρ. The function C_2 has maximum magnitude along the transition layers where $q_1 = 0$. For the WORS, the transition layers are along the diagonals and for BD, the transition layers are along a pair of parallel square edges. In particular, these transition layers have constant length independent of ρ for the BD-critical point and have length, $(1-\rho)$ for the WORS-critical point. Therefore, we can always find a v_2 such that $\delta^2 F(v_2) < 0$ for BD-critical points. In contrast, non-trivial solutions for v_2 only exist for small ρ, in the case of the WORS (see Fig. 5.9 and 5.10). Consequently, BD-critical points are always unstable in the space of $\mathcal{V}_2$ such that the perturbation W has $\mathbf{e}_z$ as a fixed eigenvector but need not have a fixed eigenframe in the (x,y)-plane.

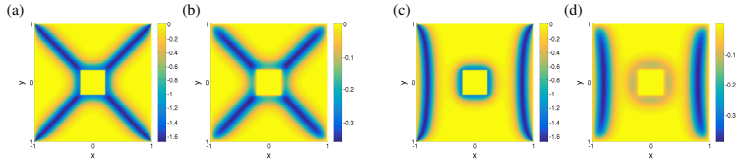

FIGURE 5.9. *(a) $C_2(x,y)$ for the WORS with $\rho = 0.2$. (b) The profile of v_2 in a perturbation s.t. $\delta^2 F(v_2) < 0$ for the WORS with $\rho = 0.2$. (c) $C_2(x,y)$ for a BD with $\rho = 0.2$. (d) The profile of v_2 in a perturbation s.t. $\delta^2 F(v_2) < 0$ for a BD with $\rho = 0.2$.*

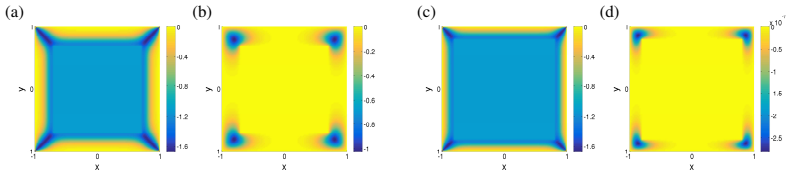

FIGURE 5.10. *(a) $C_2(x,y)$ for the WORS with $\rho = 0.7$. (b) The profile of v_2 in a perturbation s.t. $\delta^2 F(v_2) < 0$ for the WORS with $\rho = 0.7$. (c) $C_2(x,y)$ for the WORS with $\rho = 0.8$. (d) The profile of v_2 in numerical solution of (5.18) for the WORS with $\rho = 0.8$.*

Similarly, we can minimize $\delta^2 F(v_4)$ and $\delta^2 F(v_5)$ by solving the gradient flow equations

for v_4 and v_5

$$\begin{aligned} \frac{\partial v_4}{\partial t} &= 2\Delta v_4 - \bar{\lambda}^2 C_4(x,y) v_4, \\ \frac{\partial v_5}{\partial t} &= 2\Delta v_5 - \bar{\lambda}^2 C_5(x,y) v_5, \end{aligned} \tag{5.20}$$

with random initial data, where

(5.21)

$$C_4(x,y) = \frac{A}{C} - \frac{B}{C}(q_1+q_3) + 2\left(q_1^2+3q_3^2\right), \quad C_5(x,y) = \frac{A}{C} - \frac{B}{C}(q_3-q_1) + 2\left(q_1^2+3q_3^2\right).$$

The numerical solutions (for the specific parameter values in Figure 5.11 and a larger search not reported in this paper) converge to $v_4 = v_5 = 0$ for both the WORS and BD. This can be informally understood since the numerical results show that C_4 and C_5 are negative in a small region around the isotropic inclusion and from the Poincaré inequality, we cannot construct a non-trivial v_4 (or v_5) in this small region to render $\delta^2 F(v_4) < 0$ (or $\delta^2 F(v_5) < 0$).

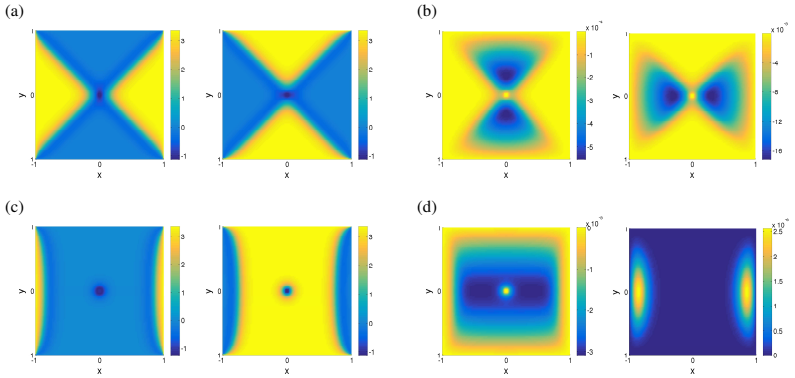

FIGURE 5.11. *(a) $C_4(x,y)$ and $C_5(x,y)$ for the WORS with $\rho = 0.02$. (b) The profiles of v_4 and v_5 in numerical solution of (5.20) for the WORS with $\rho = 0.02$. (c) $C_4(x,y)$ and $C_5(x,y)$ for a BD with $\rho = 0.02$. (d) The profiles of v_4 and v_5 in numerical solution of (5.20) for a BD with $\rho = 0.02$.*

Numerically, we find that for $A = -\dfrac{B^2}{3C}$ and $\bar{\lambda}^2 = 200$,

- the WORS is unstable over subspace $\mathcal{V}_{13}$ for small-ρ, but is stable over subspace $\mathcal{V}_{13}$ for large-ρ ($\rho \geq 0.05$). BD solutions are stable over $\mathcal{V}_{13}$ if they are critical points of the system ($\rho \leq 0.4$).
- BD solutions are unstable over subspace $\mathcal{V}_2$, the WORS is unstable over $\mathcal{V}_2$ for small-ρ, but is stable over $\mathcal{V}_2$ when ρ is large enough ($\rho \geq 0.74$).
- Both the WORS and BD are stable over subspaces $\mathcal{V}_4$ and $\mathcal{V}_5$.

The next questions are - are there any ESC-like critical points with $q_3 > 0$? BD-solutions are stable in the subspace $\mathcal{V}_{13}$ when it exists but is always unstable in $\mathcal{V}_2$. The WORS can be stable in $\mathcal{V}_2 \cup \mathcal{V}_{13}$ for either large ρ or small $\bar{\lambda}^2$, but can we identify the stable competitors for the WORS in the subspace $\mathcal{V}_2 \cup \mathcal{V}_{13}$?

5.4. Non-existence of ESC. The non-existence of ESC, at least within the restricted class of **Q**-tensors (5.6), is predicted by the Γ-convergence arguments in Section 4 and supported by solving the Euler-Lagrange equation (5.8) using the deflation technique [41]. The deflation technique enables us to discover multiple distinct

solutions of (5.8) with one initial guess. However, we haven't observed any ESC-like solutions for several different choices of the initial conditions. For $\rho = 0.2$, we find 17 critical points. Six of them remain after discarding the the rotational symmetries, as shown in Fig. 5.12(a)–(f) by the profiles of q_1. The profiles of q_3 are almost the same for all cases, see Fig. 5.12(g). Besides the WORS and BD, we find another metastable configuration in the restricted class of **Q**-tensors (5.6), shown in Fig. 5.12(c), which is between the WORS and BD (retains half the diagonal cross and one edge transition layer). The critical points shown in Fig. 5.12(d)-(f) are saddle points even in the restricted two-dimensional class.

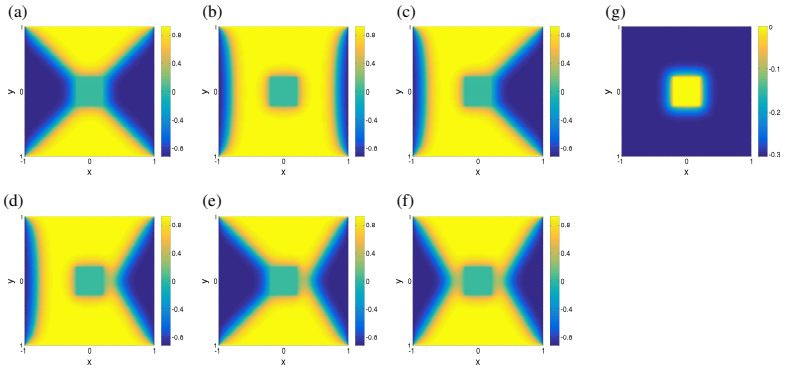

FIGURE 5.12. *(a)–(f) Critical Points with two degrees of freedom for $\rho = 0.2$ ($\bar{\lambda}^2 = 200$), shown by the profiles of q_1. (g) the profile of q_3 in all the critical points.*

For $\rho = 0.02$, we only find 3 critical points (the WORS and 2 BD-solutions), shown in Fig. 5.13. Here, the WORS is no longer a metastable state but acts as a saddle point of the system connecting two stable BD equilibria in the restricted class of **Q**-tensors (5.6).

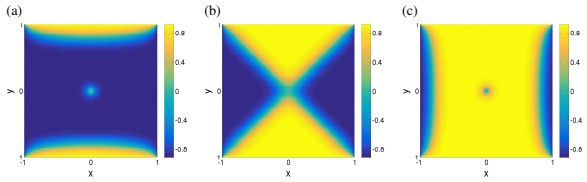

FIGURE 5.13. *Critical Points with two degrees of freedom for $\rho = 0.02$ ($\bar{\lambda}^2 = 200$), shown by the profiles of q_1.*

5.5. General Case. The critical points of the form (5.6) are a subset of LdG critical points which have two degrees of freedom. We have also calculated arbitrary critical points:

$$\begin{aligned}\mathbf{Q}(x,y) &= q_1(x,y)(\mathbf{e}_x \otimes \mathbf{e}_x - \mathbf{e}_y \otimes \mathbf{e}_y) + q_2(x,y)(\mathbf{e}_x \otimes \mathbf{e}_y + \mathbf{e}_y \otimes \mathbf{e}_x)\\ &\quad + q_3(x,y)(2\mathbf{e}_z \otimes \mathbf{e}_z - \mathbf{e}_x \otimes \mathbf{e}_x - \mathbf{e}_y \otimes \mathbf{e}_y)\\ &\quad + q_4(x,y)(\mathbf{e}_x \otimes \mathbf{e}_z + \mathbf{e}_z \otimes \mathbf{e}_x) + q_5(x,y)(\mathbf{e}_y \otimes \mathbf{e}_z + \mathbf{e}_z \otimes \mathbf{e}_y),\end{aligned} \tag{5.22}$$

which exploit all five degrees of freedom of LdG **Q**-tensor, subject to the boundary condition (5.7).

The degrees of freedom, $q_1, \dots, q_5$ (5.22), satisfy the Euler-Lagrange equation

(5.23)
$$\begin{cases} \Delta q_1 = \bar{\lambda}^2 \left(\frac{A}{2C} q_1 + \frac{B}{2C} \left(2q_1 q_3 - \frac{1}{2}(q_4^2 - q_5^2) \right) + \left(\frac{1}{2} \operatorname{tr}(\mathbf{Q}^2) \right) q_1 \right) \\ \Delta q_2 = \bar{\lambda}^2 \left(\frac{A}{2C} q_2 + \frac{B}{2C} \left(2q_2 q_3 - q_4 q_5 \right) + \left(\frac{1}{2} \operatorname{tr}(\mathbf{Q}^2) \right) q_2 \right) \\ \Delta q_3 = \bar{\lambda}^2 \left(\frac{A}{2C} q_3 + \frac{B}{2C} \left(\frac{1}{3}(q_1^2 + q_2^2) - q_3^2 - \frac{1}{6}(q_4^2 + q_5^2) \right) + \left(\frac{1}{2} \operatorname{tr}(\mathbf{Q}^2) \right) q_3 \right) \\ \Delta q_4 = \bar{\lambda}^2 \left(\frac{A}{2C} q_4 - \frac{B}{2C} \left(q_3 q_4 + q_1 q_4 + q_2 q_5 \right) + \left(\frac{1}{2} \operatorname{tr}(\mathbf{Q}^2) \right) q_4 \right) \\ \Delta q_5 = \bar{\lambda}^2 \left(\frac{A}{2C} q_5 - \frac{B}{2C} \left(q_3 q_5 - q_1 q_5 + q_2 q_4 \right) + \left(\frac{1}{2} \operatorname{tr}(\mathbf{Q}^2) \right) q_5 \right), \end{cases}$$

where $\operatorname{tr}(\mathbf{Q}^2) = 2q_1^2 + 2q_2^2 + 6q_3^2 + 2q_4^2 + 2q_5^2$.

For $\rho = 0.2$, we find 28 critical points after discarding the rotational symmetries for $\bar{\lambda}^2 = 200$, which are shown in Fig. 5.14. They all satisfy $q_4 = q_5 = 0$, have two or three degrees of freedom and have $\mathbf{e}_z$ as a fixed eigenvector, as predicted for *reduced* minimizers in Theorem 2.1. The solutions shown in panels 1-6 are as found in Fig. 5.12, which have constant eigenframes with two degrees of freedom. The solutions in panels 7-12 have no interior defects; they are distinguished by defects near vertices of topological charge $\pm\frac{1}{4}$ and are metastable in the current system. We can see interior defects with topological charge $\pm 1/2$ clearly in panels $13-28$. Unlike the case without isotropic inclusion, the total topological charges of four vertices and all interior defects can be non-zero. The solutions with interior defects are always unstable, but play important roles in the transition dynamics.

By comparing free energies of all critical points, we find that two diagonal-type solutions, one of which is shown in panel 11, has the lowest free energy for $\rho = 0.2$ and $\bar{\lambda}^2 = 200$. We have also performed simulations for $\bar{\lambda}^2 = 200$ and other values of ρ, for which the WORS is unstable. In all cases, the diagonal-type solutions are energy minimizers in the restricted class of of $\mathbf{Q}$-tensors (5.22) with $q_4 = q_5 = 0$. The numerical results suggest that the diagonal-type critical points are global minimizers of the thin systems studied in Theorem 2.1, when the WORS is unstable.

A further important numerical observation is that we haven't found any ESC-like configurations with $q_3 > 0$ around the isotropic inclusion. Actually, the profile of q_3 is almost identical for all the numerically computed critical points, as shown in Fig. 5.12(g).

For small ρ, we find two critical points with $q_4 \neq 0$ and $q_5 \neq 0$ for $\bar{\lambda}^2 = 200$, as shown in Fig. 5.15(a) and (b) for $\rho = 0.02$, by using special initial guesses. The initial condition is uniaxial around the isotropic inclusion and the leading eigenvector escapes into the third dimension around the isotropic inclusion with winding number ± 1. The resulting critical points are almost uniaxial around the isotropic inclusion with $q_3 > 0$ (also see Fig. 5.15(c)-(h)). These two types of critical points are metastable in the system whenever they exist, but have higher free energy than diagonal-type solutions. These critical points do not exist for relatively large ρ ($\rho > 0.052$ as indicated by 5.15(i)). We do not analyse this further in this paper, largely because these escaped critical points seem rare for this model problem. We expect these escaped critical points to occur more frequently for three-dimensional systems and not for severely confined systems such as those considered in this manuscript.

6. Conclusion. We study LdG critical points inside a three-dimensional square well with an isotropic square inclusion, with tangent Dirichlet boundary conditions

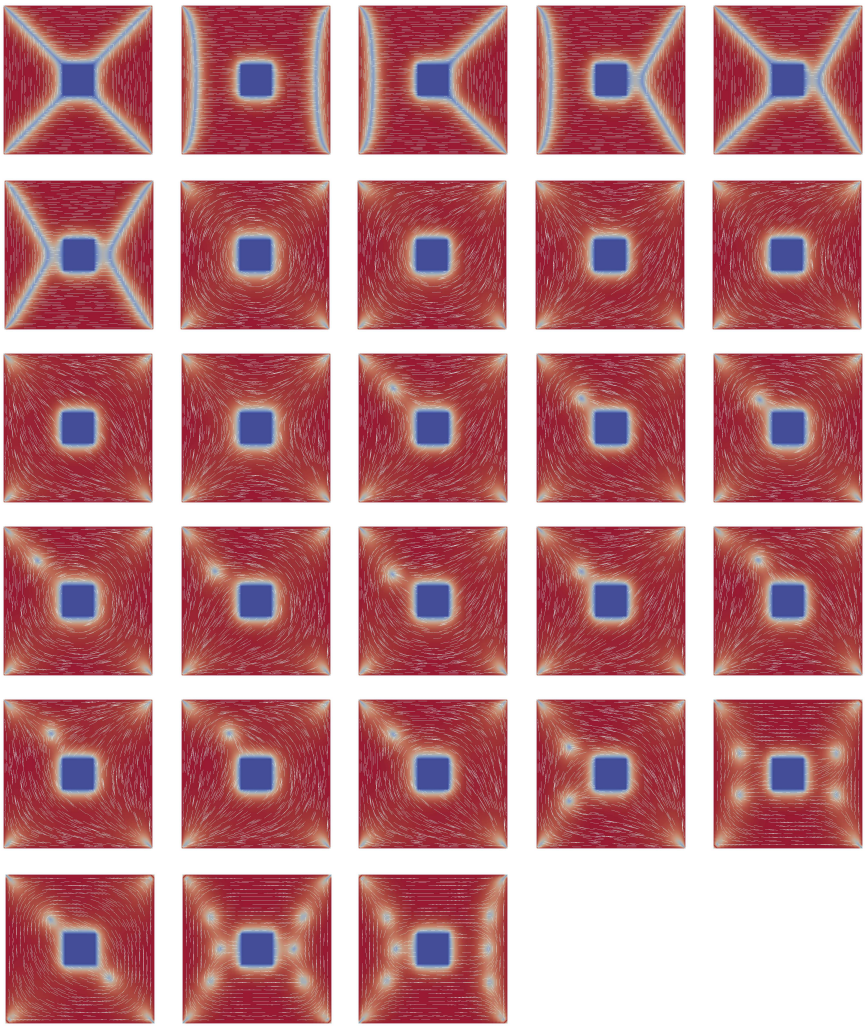

FIGURE 5.14. *Critical Points found by deflation techniques for* $\rho = 0.2$ *(*$\bar{\lambda}^2 = 200$*), which are shown by the largest eigenvalue of* $\mathbf{Q}$ *(the colors are arranged such that the high to low values correspond to variations from red to blue) and the corresponding eigenvector.*

on the lateral surfaces and surface anchoring energies that enforce planar degenerate conditions, on the top and bottom surfaces, in the thin film limit. In three-dimensions, the inclusion would be an isotropic interior pillar with a square cross-section. In Theorem 2.1, we adapt arguments from [44] to reduce this three-dimensional study to a two-dimensional study on the square cross-section with an isotropic square hole (inclusion). We prove the existence of a WORS-type critical point, featured by a distinctive negatively ordered uniaxial cross along the diagonals, connecting the vertices of the inner and outer squares. We partition LdG critical points into three categories: critical points with two degrees of freedom which have a constant eigenframe (to which the WORS and BD solutions belong), critical points with three degrees of freedom which have $\mathbf{e}_z$ as a fixed eigenvector but variable eigenvectors in the (x, y)-plane (within the remit of Theorem 2.1) and critical points which exploit all five degrees of freedom.

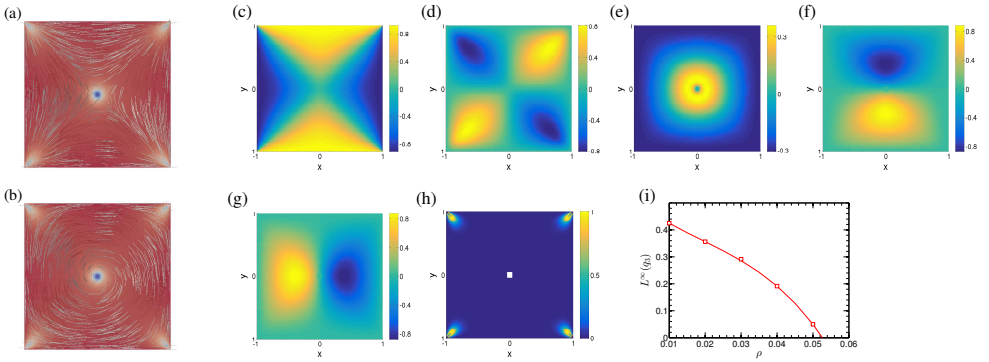

FIGURE 5.15. *(a)-(b) Two critical points with $q_4 \neq 0$ and $q_5 \neq 0$ for $\rho = 0.02$, shown by the largest eigenvalue of* $\mathbf{Q}$ *(the colors are arranged such that the high to low values correspond to variations from red to blue) and the corresponding eigenvector. (c)-(h) The profiles of q_i and β^2 in configuration(a). (i) $||q_3||_{L^\infty}$ as the function of ρ in configuration (a).*

In the two-dimensional sub-class, there are effectively three competitors: the WORS configuration, the BD configuration with negatively-ordered uniaxial transition layers along a pair of opposite square edges and a third configuration somewhere in between the WORS and the BD (retains half the diagonal cross and one edge transition layer). The WORS typically loses stability with respect to BD-type solutions in the two-dimensional setting as the square size increases or as the aspect ratio of the domain decreases. The WORS is globally stable with respect in certain parameter regimes but the BD is never stable with respect to in-plane perturbations. In fact, the in-plane perturbations are the most effective in de-stabilizing either the WORS or BD critical points, which can be intuitively understood since these perturbations distort the eigenvectors in the square plane to reduce the elastic energy (the Dirichlet energy density term in (2.10)). We carry out a fairly exhaustive study of the LdG critical points in the reduced three-dimensional setting and recover up to twenty eight critical points for $\bar{\lambda}^2 = 200$ and $\rho = 0.2$. **For moderately large values of the square size and small aspect ratios which render the WORS unstable, the numerically computed locally stable solutions have no interior defect, such as diagnoal and rotated solutions. The diagonal solution is the energy minimizer in this reduced three-dimensional setting when the WORS is unstable, within the remit of our numeric.** The diagonal and rotated solutions have been studied extensively in a batch of papers [6, 3, 7]; informally speaking, the corresponding LdG $\mathbf{Q}$-tensor can be written as

$$\mathbf{Q} = q\left(\mathbf{a}(x,y)\otimes\mathbf{a}(x,y) - \mathbf{I}_2/2\right) + q_3\left(2\mathbf{e}_z\otimes\mathbf{e}_z - \mathbf{e}_x\otimes\mathbf{e}_x - \mathbf{e}_y\otimes\mathbf{e}_y\right),$$

where $\mathbf{a}$ is an inhomogeneous unit-vector in the square plane (e.g. pointing along one of the diagonals for the diagonal state) and $\mathbf{I}_2 = \mathrm{diag}(1,1,0)$. These solutions necessarily have three degrees of freedom. For the model problem studied here, we do not expect to have stable critical points with full five degrees of freedom, as indicated by Theorem 2.1. We will study LdG critical points on a three-dimensional rectangular box, where the vertical dimension is much smaller than the cross-sectional dimension, and then gradually increase the vertical dimension to check the stability of the WORS with respect to out-of-plane perturbations.

7. Acknowledgments. Y.W. thanks the University of Bath and Keble College for their hospitality, he thanks his Ph.D. advisor Professor Pingwen Zhang, for his constant support and helpful advice. G.C.'s research was supported by the Basque Government through the BERC 2018-2021 program; by the Spanish Ministry of Science, Innovation and Universities: BCAM Severo Ochoa accreditation SEV-2017-0718; and by the Spanish Ministry of Economy and Competitiveness: MTM2017-82184-R. A.M. was supported by fellowships EP/J001686/1 and EP/J001686/2, is supported by an OCIAM Visiting Fellowship and the Keble Advanced Studies Centre. She also thanks the Chinese Academy of Sciences and the Banff International Research Station for relevant collaborative opportunities. The authors thank Professor Paul Milewski for helpful discussions about the numerics.

REFERENCES

[1] P. G. De Gennes and J. Prost. *The Physics of Liquid Crystals*. Clarendon Press, Oxford, 1974.
[2] E. G. Virga. *Variational Theories for Liquid Crystals*, volume 8 of *Applied Mathematics and Mathematical Computation*. Chapman & Hall, London, 1994.
[3] C. Tsakonas, A. J. Davidson, C. V. Brown, and N. J. Mottram. Multistable alignment states in nematic liquid crystal filled wells. *Appl. Phys. Lett.*, 90(11), 2007.
[4] S. Kralj and A. Majumdar. Order reconstruction patterns in nematic liquid crystal wells. *Proc. R. Soc. Lond. Ser. A Math. Phys. Eng. Sci.*, 470(2169):20140276, 18, 2014.
[5] C. Anquetil-Deck, D. J. Cleaver, and T. J. Atherton. Competing alignments of nematic liquid crystals on square-patterned substrates. *Phys. Rev. E*, 86:041707, Oct 2012.
[6] C. Luo, A. Majumdar, and R. Erban. Multistability in planar liquid crystal wells. *Phys. Rev. E*, 85:061702, Jun 2012.
[7] A. Lewis, I. Garlea, J. Alvarado, O. Dammone, O. Howell, A. Majumdar, B. Mulder, M. P. Lettinga, G. Koenderink, and D. Aarts. Colloidal liquid crystals in rectangular confinement: Theory and experiment. *Soft Matter*, 39(10):7865–7873, October 2014.
[8] N. Schopohl and T. J. Sluckin. Defect core structure in nematic liquid crystals. *Phys. Rev. Lett.*, 59:2582–2584, 1987.
[9] E. Penzenstadler and H.-R. Trebin. Fine structure of point defects and soliton decay in nematic liquid crystals. *J. Phys. (Paris)*, 50(9):1989, 1027–1040.
[10] S. Mkaddem and E. C. Gartland. Fine structure of defects in radial nematic droplets. *Phys. Rev. E*, 62:6694–6705, Nov 2000.
[11] P. Palffy-Muhoray, E. C. Gartland, and J.-R. Kelly. A new configurational transition in inhomogeneous nematics. *Liq. Cryst.*, 16(4):713–718, 1994.
[12] F. Bisi, E. C. Gartland, R. Rosso, and E. G. Virga. Order reconstruction in frustrated nematic twist cells. *Phys. Rev. E*, 68:021707, Aug 2003.
[13] F. Bisi, E. G. Virga, and G. E. Durand. Nanomechanics of order reconstruction in nematic liquid crystals. *Phys. Rev. E*, 70:042701, Oct 2004.
[14] X. Lamy. Bifurcation analysis in a frustrated nematic cell. *J. Nonlinear Sci.*, 24(6):1197–1230, 2014.
[15] H. Dang, P. C. Fife, and L. A. Peletier. Saddle solutions of the bistable diffusion equation. *Z. Angew. Math. Phys.*, 43(6):984–998, 1992.
[16] M. Schatzman. On the stability of the saddle solution of Allen-Cahn's equation. *Proc. Roy. Soc. Edinburgh Sect. A*, 125(6):1241–1275, 1995.
[17] M. Robinson, C. Luo, A. Majumdar, and R. Radek Erban. Front Propagation at the Nematic-Isotropic Transition Temperature. In preparation, 2016.
[18] R. S. Palais. The principle of symmetric criticality. *Comm. Math. Phys.*, 69(1):19–30, 1979.
[19] Y. Yi, M. Nakata, R. Martin, Alexander and A. Clark, Noel Alignment of liquid crystals by topographically patterned polymer films prepared by nanoimprint. Applied physics letters, 2007, 90, 163510.
[20] Y. Yi, G. Lombardo, N. Ashby, R. Barberi, J. E. Maclennan, and N. A. Clark. Topographic-pattern-induced homeotropic alignment of liquid crystals. Phys. Rev. E, 79:041701, 2009.
[21] A. H. Lewis, I. Garlea, J. Alvarado, O. J. Dammone, P. D. Howell, A. Majumdar, B. M. Mulder, M. Lettinga, G. H. Koenderink and D. G. Aarts. Colloidal liquid crystals in rectangular confinement: theory and experiment. Soft Matter, 2014, 10, 7865–7873.
[22] M. Slavinec, E. Klemenčič, M. Ambrožič, and M. Krašna. Order reconstruction in a nanoconfined nematic liquid crystal between two coaxial cylinders. Materials, 8(12):8072–8086,

2015.
[23] X. Zhou, Z. Zhang, Q. Zhang and W. Ye. Order reconstruction in a nanoconfined nematic liquid crystal between two coaxial cylinders. Materials, 8(12):8072–8086, 2015.
[24] I. C. Gârlea, P. Mulder, J. Alvarado, O. Dammone, D. G. A. L. Aarts, M. P. Lettinga, G. H. Koenderink and B. M. Mulder, Finite particle size drives defect-mediated domain structures in strongly confined colloidal liquid crystals. Nature communications, 7:12112, 2016.
[25] A. Majumdar. Equilibrium order parameters of nematic liquid crystals in the Landau-de Gennes theory. *Eur. J. Appl. Math.*, 21(2):181–203, 2010.
[26] L. C. Evans. *Partial Differential Equations*, volume 19 of *Graduate Studies in Mathematics*. American Mathematical Society, Providence, RI, second edition, 2010.
[27] A. Majumdar and A. Zarnescu. Landau-De Gennes theory of nematic liquid crystals: the Oseen-Frank limit and beyond. *Arch. Ration. Mech. Anal.*, 196(1):227–280, 2010.
[28] L. Modica and S. Mortola. Il limite nella Γ-convergenza di una famiglia di funzionali ellittici. *Boll. Un. Mat. Ital. A (5)*, 14(3):526–529, 1977.
[29] P. Sternberg. The effect of a singular perturbation on nonconvex variational problems. *Arch. Rational Mech. Anal.*, 101(3):209–260, 1988.
[30] A. Braides. A handbook of Γ-convergence. volume 3 of *Handbook of Differential Equations: Stationary Partial Differential Equations*, pages 101–213. North-Holland, 2006.
[31] P. Grisvard. *Elliptic problems in nonsmooth domains*, volume 24 of *Monographs and Studies in Mathematics*. Pitman (Advanced Publishing Program), Boston, MA, 1985.
[32] D. Gilbarg and N. S. Trudinger. *Elliptic partial differential equations of second order*. Classics in Mathematics. Springer-Verlag, Berlin, 2001. Reprint of the 1998 edition.
[33] F. Bethuel, H. Brezis, and F. Hélein. Asymptotics for the minimization of a Ginzburg-Landau functional. *Calc. Var. Partial Dif.*, 1(2):123–148, 1993.
[34] M. G. Crandall and P. H. Rabinowitz. Bifurcation from simple eigenvalues. *J. Functional Analysis*, 8:321–340, 1971.
[35] M. G. Crandall and P. H. Rabinowitz. Bifurcation, perturbation of simple eigenvalues and linearized stability. *Arch. Rational Mech. Anal.*, 52:161–180, 1973.
[36] M. A. Peletier. Energies, gradient flows, and large deviations: a modelling point of view. 2011.
[37] A. Majumdar, P. A. Milewski, and A. Spicer. Front Propagation at the Nematic-Isotropic Transition Temperature. Preprint arXiv: 1505.06143, 2016.
[38] S. Baldo. Minimal interface criterion for phase transitions in mixtures of Cahn-Hilliard fluids. *Ann. Inst. H. Poincaré Anal. Non Linéaire*, 7(2):67–90, 1990.
[39] I. Fonseca and L. Tartar. The gradient theory of phase transitions for systems with two potential wells. *Proc. Roy. Soc. Edinburgh Sect. A*, 111(1-2):89–102, 1989.
[40] A. Iserles. A first course in the numerical analysis of differential equations. Cambridge university press, 2009.
[41] P. E. Farrell, A. Birkisson, and S. W. Funke. Deflation techniques for finding distinct solutions of nonlinear partial differential equations. *SIAM J. Sci. Comput.* 37-4:A2026–A2045,2015.
[42] M. Robinson, C. Luo, P. E. Farrell, R. Erban and A. Majumdar. From molecular to continuum modelling of bistable liquid crystal devices. Liquid Crystals 44(14-15), 2267-2284, 2017.
[43] G. Canevari, A. Majumdar and A. Spicer. Order reconstruction for nematics on squares and regular polygons: A Landau-de Gennes study. *SIAM J. Appl. Math.* 77(1):267–293, 2017.
[44] D. Golovaty, J. Montero and P. Sternberg. Dimension reduction for the Landau-de Gennes model in planar nematic thin films. *J. Nonlinear Sci.* 25:1431, 1451, 2015.
[45] M. R. Novack, Dimension reduction for the Landau-de Gennes model: The vanishing nematic correlation length limit. To appear in *SIAM J. Math. Anal.* Preprint arXiv 1801.04477
[46] L. Simon. *Lecture on Geometric Measure Theory*. Proceedings of the Centre for Mathematical Analysis. Australian National University, Centre for Mathematical Analysis, Canberra, 1983.
[47] M. P. do Carmo. *Riemannian geometry*. Mathematics: Theory & Applications. Birkhäuser Boston Inc., Boston, MA, 1992. Translated from the second Portuguese edition by Francis Flaherty.
[48] A. P. G. Robinson, R. E. Palmer T. Tada, T. Kanayama, M. T. Allen, J. A. Preece and K. D. M. Harris. 10 nm scale electron beam lithography using a triphenylene derivative as a negative/positive tone resist. J. Phys. D: Appl. Phys. 32 L75, 1999.